Journal of MATERIALS RESEARCH

Invited Feature Paper-Review
DOI:10.1557/s43578-022-00646-7

MULTISCALE CHARACTERIZATION AND ANALYSIS FOR UNDERSTANDING ENERGY STORAGE MECHANISMS IN RECHARGEABLE BATTERIES

FOCUS ISSUE

Critical overview of polyanionic frameworks as positive electrodes for Na-ion batteries

Debolina Deb[1], Gopalakrishnan Sai Gautam[1,a)]

[1] Department of Materials Engineering, Indian Institute of Science, Bengaluru 560012, India
[a)] Address all correspondence to this author. e-mail: saigautamg@iisc.ac.in

Received: 1 March 2022; accepted: 29 June 2022

Na-ion batteries (NIBs) are an important technological alternative to Li-ion batteries (LIBs) for developing energy storage systems that are cost-effective and less constrained by geographical supply chains, with similar energy densities. Analogous to LIBs, cathodes play a critical role in determining the energy density of NIBs, and layered transition metal oxide compounds are widely used as NIB cathodes. However, the instability-driven irreversible phase transitions in layered frameworks, especially at large degrees of Na removal, has necessitated the exploration of rigid structural frameworks that are resistant to structural changes with Na exchange. Thus, polyanionic frameworks, which primarily consist of transition metal polyhedra interconnected by PO_4, SiO_4, and/or SO_4 units, with or without the presence of fluorine, have been investigated as NIB cathodes. This review provides a critical overview of recent studies using polyanion cathodes, which will be useful in guiding the scientific community towards the development of better NIB cathodes.

Introduction

Ensuring a sustainable future, in terms of utilizing carbon-free energy generation and distribution that satisfies the climate-change goals established in the Paris agreement, requires the development of cost-effective, energy-dense, and safe energy storage systems. The state-of-the-art (SOTA) in energy storage technology is the lithium ion battery (LIB) system, which has captured the dominant market share in portable electronics and electric vehicles, with increasing deployment in grid-scale energy storage as well as aviation [1–5]. The success of LIBs so far can be largely attributed to their high gravimetric and volumetric energy density, ~ 100–265 Wh kg^{-1} and ~ 250–670 Wh l^{-1}, respectively, which is facilitated by the graphite anode (theoretical gravimetric capacity of 372 mAh g^{-1} of graphite) [6, 7]. However, LIBs are reaching the fundamental limits of energy density that can be achieved [8, 9], besides geopolitical constraints surrounding the supply of key metals (Li, Co, etc.), and safety issues (owing to oxygen evolution and/or lithium dendrite growth) [10].

An alternative to LIB is the sodium ion battery (NIB) system, which employs Na as the electroactive species in place of Li. The abundance of Na available on the earth's crust ensures markedly lower price of the Na_2CO_3 precursor used for NIB compared to Li_2CO_3 used for LIBs (Na_2CO_3, \$150 ton^{-1}; Li_2CO_3, \$5000 ton^{-1}) [11]. Moreover, NIBs utilize similar engineering and production methods as the well-established protocols in LIBs, in addition to using cheaper Al (vs. Cu in LIB) current collectors [12]. Additionally, NIBs typically exhibit better thermal stability than LIBs owing to their lower self-heating rate [7, 13]. However, the biggest disadvantage of NIBs is the lower (i.e., more positive) reduction potential of Na metal (– 2.7 V vs. standard hydrogen electrode—SHE), compared to Li's – 3.4 V vs. SHE, which typically causes an associated decrease in the average voltages exhibited and a reduction in the energy density [14]. The rate performance of NIBs, besides energy density, also needs improvement to compete better with LIBs [15]. In any case, innovations in the materials being used, as the intercalation electrode and the electrolyte, and cell design optimization strategies can enable NIBs to overcome its intrinsic drawbacks and capture a significant market share among energy storage technologies in the near future.

In this work, we review some of the recent developments that have taken place in the positive electrode or cathode space of NIBs. Similar to LIBs, cathodes in NIBs significantly influence both energy and power performance of the full electrochemical system, and hence require significant improvements. Note that

NIBs also need an anode that is as functional (or better) than graphite in LIBs, and the search for better anodes continues to be an active area of research [16]. Nevertheless, a search for cathodes can occasionally lead to the discovery of high capacity and low operating voltage materials that can be used as anodes. The SOTA of Na-ion intercalation cathodes are the layered transition metal (TM) oxide frameworks (see "Layered oxides" section for additional details) [17], which typically exhibit high energy densities, good electronic conductivity, but suffer from irreversible structure transitions upon electrochemical cycling. Prussian blue analogs are another class of potential cathodes that have been explored for NIBs but require further improvements in energy densities for being employed in commercial devices [18, 19]. On the other hand, polyanionic frameworks, such as those based on silicate, phosphate, sulfate, etc., moieties, with or without fluorine, are being actively explored as Na cathodes [20], with the structural integrity upon Na (de)intercalation being their distinct advantage. Thus, we review the different chemical and structural classes of polyanionic frameworks that have been explored experimentally and/or theoretically as Na-ion cathodes. While previous reviews on Na-ion cathodes [21], especially on layered oxides [17, 22], and specific polyanionic structures [23–25] exist, our aim is to provide an overview of several types of polyanionic hosts that have been explored as Na cathodes.

We begin with a brief summary of layered oxides as Na intercalation cathodes in "Layered oxides" section. Subsequently, we focus on an individual structural/mineral type of a polyanionic framework in the following sections, with differences in chemistry (e.g., differences in TM/polyanionic moiety employed) included within each section. For example, we review the natrium superionic conductor (NaSICON)-class of cathodes in "NaSICONs" section, olivines and other ortho-polyanionic hosts in "Olivines and ortho-polyanions" section, alluaudites in "Alluaudites" section, and pyrophosphates in "Pyrophosphates" section. In "Fluoro-polyanions" and "Perovskites and rutiles" sections, we focus on fluorine-containing oxide frameworks, such as fluoro-polyanions, perovskites, and rutile structures. In each section, we describe the polymorphism and the structural features of each cathode framework, followed by a summary of the electrochemical performance that has been measured and/or predicted. While reporting electrochemical performance, we do not explicitly summarize doping, nanosizing, and/or carbon-coating-based performance enhancements [26, 27], since these techniques typically do not fundamentally alter the bulk electrode properties. Wherever applicable, we also provide our critical outlook on electrochemical measurements and/or theoretical calculations that have been performed so far to further accelerate future materials design. In the final section, we provide a summarizing table of some of the cathode frameworks that appear promising (within each structural/mineral type) followed by a few concluding remarks.

Throughout this review, we have strived to report the relevant intercalation voltages, in units of V versus Na metal (i.e., versus Na^+/Na), in terms of the average voltage, the open circuit voltage (OCV), or the voltage range across which the electrochemical charge/discharge has been performed. We also report the observed electrochemical capacities (in units of mAh g^{-1}), the cycling performance (number of cycles, with or without % capacity fade/retention), and the rate performance (in terms of C-rate or A g^{-1} or mA cm^{-2}). We have also included energy density (in units of Wh kg^{-1} or Wh l^{-1}), in case they have been explicitly reported. Besides experimental studies, theoretical or computational works, often utilizing density functional theory (DFT [28, 29])-based calculations, report average Na intercalation voltages (in units of V vs. Na) and/or the predicted phase behavior upon Na (de)intercalation in a cathode framework. Additionally, some theoretical studies do report activation barriers for Na migration in candidate cathode hosts (in units of eV or meV), usually computed with accurate ab initio molecular dynamics (AIMD [30])/DFT-nudged elastic band (DFT-NEB [31]) or the swifter bond valence site energy (BVSE [32]) calculations, which aid in characterizing Na transport. The experimental techniques usually employed to study Na diffusion are variable temperature impedance spectroscopy and/or variable temperature nuclear magnetic resonance [33, 34], with ionic conductivities (in units of mS cm^{-1}) and/or migration barriers (eV or meV) reported. The intended audience for this review are the computational and experimental researchers working on battery systems in general, and NIBs in particular, and we hope that our work will provide a timely summary of the latest progress that has been made and facilitate an accelerated development of commercial-scale NIBs.

Layered oxides

The layered oxide framework is at the forefront of commercial LIB technology, with the cathode of choice being either layered lithium cobalt oxide ($LiCoO_2$) or a layered oxide framework with mixed metals (e.g., Ni–Mn–Co or Ni–Co–Al besides Li) [8]. Stoichiometric layered oxides exhibit a general formula of A_xMO_2, where A is the electroactive cation (Li or Na), M is the TM and x denotes the amount of alkali ion ($x = 1$ for a stoichiometric compound). The robust performance of layered oxide cathodes in LIBs has resulted in this class of compounds being the most widely studied as Na cathodes as well, and consequently, represent the SOTA cathodes in NIBs [35]. Indeed, cathodes used in commercial NIBs, as manufactured by Faradion®, are based on layered TM oxides [15]. The layered framework can exhibit several different phases (with unique Na-vacancy orderings), such as O3, P3, and P2 characterized by the coordination environment exhibited by Na (octahedral or O, and prismatic or P), the Na content present in the structure,

and the stacking sequence of the oxygen layers. A compilation of the different phases that occur within Na-containing layered oxides involving 3*d* TMs is provided in Table 1. Note that the co-existence of several layered phases can also result in the existence of stacking faults [35] during Na (de)intercalation.

Several stoichiometric $NaMO_2$ compounds exhibit the O3 structure, where the oxygen sub-lattice is a face-centered-cubic (FCC) framework, providing octahedral sites for TM and Na occupation and tetrahedral voids between occupied octahedral sites [Fig. 1(a)]. Layers of oxygen atoms (along the {111} planes of the FCC framework) assemble in a "-A_B-C_A-B_C-" stacking sequence, where Na and M ions occupying edge-shared octahedral sites between oxygen layers are represented by "_" and "-", respectively. In the O3 structure, the periodicity of the oxygen stacking is restored after every sixth oxygen layer, i.e., after accommodating three pairs of alternating MO_6 and NaO_6 slabs, resulting in an $R\bar{3}m$ symmetry [36]. Thus, the term O3 signifies the octahedral environment for Na and the presence of three slabs of MO_6 octahedra in the $R\bar{3}m$ unit cell. Notably, $NaMO_2$ compounds, with M = Ti, V, Cr, Fe, and Co, exhibit the $R\bar{3}m$ O3 structure, while the Mn and Ni analogs adopt the monoclinic O'3 structure (with $C2/c$ space group), due to the Jahn–Teller distortions of Mn^{3+} and Ni^{3+} [37–39]. Likewise, the Mo analog, $NaMoO_2$, crystallizes in a triclinically-distorted O″3 structure due to the formation of "diamond-like" Mo-clusters, with the structure displaying reversible exchange of half a mole of Na per MoO_2 formula unit [40].

O3 phases can show a transition to a P3 phase during Na deintercalation from $NaMO_2$, particularly around half desodiation, where the Na ions occupy prismatic instead of octahedral sites [Fig. 1(b)]. The Na occupation of prismatic sites is facilitated by the glide of oxygen layers, over the MO_2 slab, indicating that the O3-P3 transition does not involve breaking of any M–O bonds. Notably, P3-Na_xMO_2 follows an oxygen layer stacking sequence of -A_B-B_C-C_A- and exhibits three MO_2 slabs in the $R\bar{3}m$ unit cell. The prismatic NaO_6 shares a face with a MO_6 octahedra of one MO_2 slab and edges with three other MO_6 octahedra of the adjacent MO_2 slab [Fig. 1(b)]. While the P3 structure has twice as many prismatic sites as MO_6 octahedral sites, not all prismatic sites can be simultaneously occupied owing to Na^+–Na^+ electrostatic repulsions, often resulting in a "honeycomb" arrangement of occupied Na sites [41]. Analogous to O′3, a monoclinically distorted version of P3, namely P′3, can also exist [42]. Among 3*d* Na_xMO_2, Cr, Mn, Co, and Ni exhibit a O3 (or O′3)-P3 (or P′3) transition [37, 38, 43, 44], which can be attributed to the stability of the prismatic ordering upon desodiation [35, 45]. For $x < ½$ in Na_xMO_2, both P3 and O3 are feasible within the layered framework, apart from O1 and staged-hybrid structures [46, 47].

P2 is another phase exhibited by layered transition metal oxides when the as-synthesized material, Na_xMO_2, has partial sodium content usually within $x \sim 0.5$–0.8 [48–50]. Unlike P3, P2 has oxygen layer stacked in a -A_B-B_A- sequence, resulting in a $P6_3/mmc$ hexagonal unit cell [Fig. 1(c)]. There are two types of Na prismatic sites in P2, namely those that shares edges with MO_6 octahedra along both MO_2 slabs adjacent to Na, and those that share faces with both adjacent MO_6 octahedra, with the former being typically preferred due to lower Na–M electrostatic repulsions [51]. Note that the P2 phase cannot be obtained via glide transitions (i.e., without M–O bond breakage) from O3/P3 phases. Hence, P2 cannot be electrochemically obtained from O3/P3 structures, especially at room temperature [52]. Among 3*d* TM oxides, stable P2-$Na_{0.67}MO_2$ could be experimentally prepared only for M = V, Mn, and Co [48–50, 53]. P2 frameworks can transition into O2 structures upon change in Na via gliding of oxygen layers [54], similar to the O3-P3 transition. O2 phase displays a -A_B-A_C- oxygen stacking sequence and the $P6_3/mmc$ space group. The P2-O2 transition is usually common in mixed-TM oxides compared to single-TM oxides, upon electrochemical charging.

TABLE 1: Phases observed in layered single-TM oxides during charge–discharge electrochemical cycling.

Comp	O3	O′3	P′3	P3	P2	Capacity @ rate	Voltage	References
Na_xTiO_2	**0.76 < x < 1**	0.5 < *x* < 0.72				152 @ 0.1	0.6–1.6	[61]
Na_xVO_2	**x ~ 1**	0.5 < *x* < 0.67			**0.47 < x < 0.92**	~125 @ 0.05 (O3/O′3) ~122 @ 0.05 (P2)	1.2–2.4	[48]
Na_xCrO_2	**0.91 < x < 1**	~ 0.8 < *x* < 0.83	~ 0.17 < *x* <~ 0.71			110 @ 0.05	2.5–3.6	[43]
Na_xMnO_2		**~ 0.7 < x < 1**			**0.45 < x < 0.85**	185 @ 0.1 (O′3) 140 (P2)	2.0–3.8	[37, 49]
Na_xFeO_2	**x ~ 1**	*x* ~ 0.5				80–100	2.5–3.5	[62]
Na_xCoO_2	**x = 1**	0.81 < *x* < 0.88	0.59 < *x* < 0.67; *x* <~ 0.54	*x* = 0.56	**0.68 < x < 0.76**	~130 @ 0.05 (O3) 121 @ 0.1 (P2)	2.5–3.5 (O3) 2.0–4.2 (P2)	[44, 50]
Na_xNiO_2		**x = 1**	*x* = 0.70			114.6@0.1	1.5–4.0	[38]

An overall summary of electrochemical properties of each composition is also provided in terms of the practical capacity (in mAh g^{-1}) at rate (in C-rate), and voltage range of operation (in V vs. Na). Boxes with text in bold font mark the starting phase(s) used in electrochemical cycles.

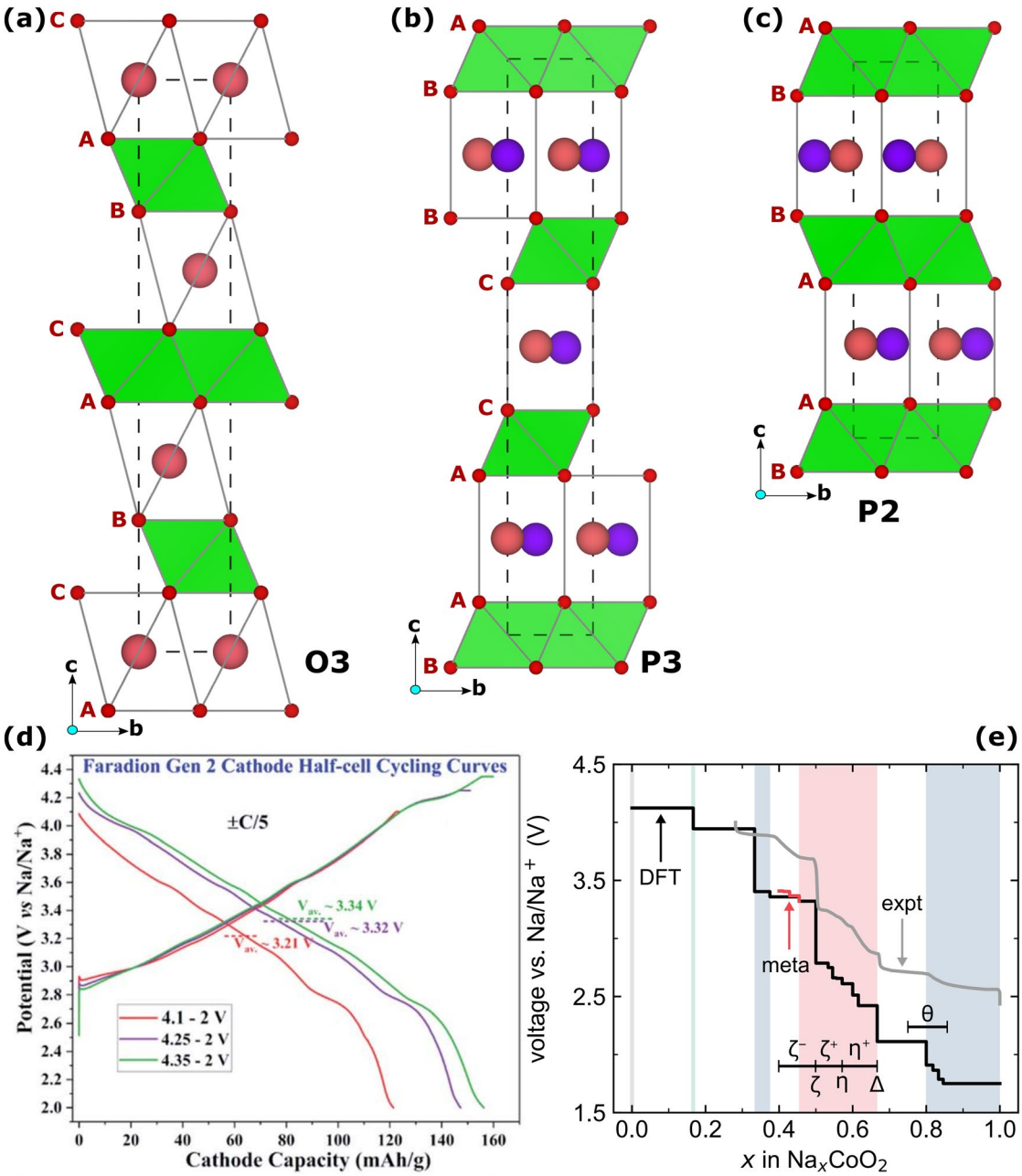

Figure 1: Conventional unit cells of (a) O3-, (b) P3-, and (c) P2-stacked Na-containing layered TM oxides. Green polyhedra indicate TM sites with red spheres corresponding to O atoms. Pink/purple spheres indicate Na sites, with solid black lines highlighting the coordination environment of Na. Dashed black lines signify the boundaries of the conventional cell. (d) Half-cell electrochemical performance of the O3 + P2 layered cathode ("Gen 2") over different voltage ranges. Figure modified from Ref. [15], copyright 2021 Royal Society of Chemistry. (e) DFT-calculated (solid black line) and experimental (solid gray line) Na intercalation voltage in O3/P3-Na_xCoO_2 as a function of Na content (x). The calculated voltage profile is also an illustration of the "devil's staircase". Figure reproduced from Ref. [46], copyright 2019 American Physical Society.

Apart from the orderings mentioned above, Na-containing layered oxides can exhibit other phases such as OP4 and P′2 which are observed in certain mixed-TM oxide chemistries [55, 56]. With respect to Na migration in layered oxides, prismatic phases generally show more facile Na transport compared to octahedral [57]. This is because, Na migration in octahedral phases occurs via an intermediate tetrahedral site, which is typically face-sharing with a MO_6 octahedron and suffers from electrostatic repulsions, resulting in higher barriers. However, Na migration barriers can also change significantly, in both O3 and P2 phases, depending on Na content [57].

In terms of electrochemical performance, layered single-TM oxides can display a capacity in the range of 80–185 mAh g^{-1} (see Table 1) at 0.05–0.2 C, with O3 phases typically showing marginally higher capacities than P2, owing to higher Na content present in the cathode (i.e., O3-$NaMO_2$ vs. P2-$Na_{0.67}MO_2$). The voltage ranges that layered oxides can be cycled across can vary between 0.6 and 1.6 V vs. Na in Na_xTiO_2 to 1.5–4.0 V vs. Na in Na_xNiO_2, depending on the structure (O3/P2) and the redox couple of the TM (see Table 1). However, O3-type materials often display a voltage profile with several plateaus and steps, referred to as the "devil's staircase" [Fig. 1(e)] [46], caused by irreversible lattice-invariant shear transitions eventually giving rise to "electrochemical creep" [47]. On the other hand, P2 phases typically exhibit single solid solution regions that are separated by either voltage plateaus or steps [58], and usually show low degrees of polarization between charge and discharge curves, but are prone to irreversible phase changes when cycled over 4 V vs. Na [59]. Note that both O3 and P2 structures are prone to significant lattice strains due to desodiation, which can result in defective layered frameworks upon electrochemical cycling [47].

Layered frameworks with multiple TMs do exhibit better electrochemical performance compared to single-TM structures [60]. Moreover, layered frameworks that can exhibit multiple phases simultaneously (e.g., O3 + P2) can offset the lattice strains due to Na addition/removal [15]. Indeed, a combination of O3-$NaNi_{0.333}Mn_{0.333}Mg_{0.167}Ti_{0.167}O_2$ and P2-$Na_{0.667}Ni_{0.3}Mn_{0.6}Mg_{0.033}Ti_{0.067}O_2$ delivered a maximum ~ 156 mAh g^{-1} capacity when cycled between 4.35 and 2 V voltage window at 0.2 C [Fig. 1(d)] [15]. However, the capacities of the above O3 + P2 multi-phase cathode does drop significantly (to ~ 101 mAh g^{-1}) when the voltage range is limited to 4–1 V vs. Na. In terms of cycle life, the O3 + P2 cathode can perform up to 3000 cycles with a ~ 20% capacity fade at 1 C [15], indicating robust performance.

In summary, layered oxide frameworks are indeed the SOTA cathodes in NIBs, with modern battery architectures achieving energy densities of ~ 140 Wh kg^{-1}, which is comparable to the 137 Wh kg^{-1} typically achieved in $LiFePO_4$-based LIBs, but lower than layered oxide-based LIBs (~ 260 Wh kg^{-1}) [15]. Layered oxides also display robust cyclic performance at low rates (< 1 C), while fast-rate cycling (4 C or above) is still a work in progress [15]. However, given the irreversible phase transitions that can occur via invariant lattice-shear [35] (due to stacking sequence changes and lattice strains due to Na addition/removal), particularly at high voltages (~ 4 V vs. Na), layered oxide frameworks are unlikely to go beyond the energy densities exhibited by LIBs and may not exhibit as robust a cycling performance as LIBs. Hence, to achieve higher energy densities, frameworks that can yield higher voltages than layered analogs, without exhibiting significant lattice strains upon (de)sodiation, such as polyanionic materials, need to be developed. In the subsequent sections, we describe some of the polyanionic frameworks that have been explored as Na intercalation cathodes.

NaSICONs

NaSICONs were first characterized by Goodenough and Hong in the 1970s as frameworks that exhibited swift Na mobility. The classical NaSICON, $Na_xZr_2Si_{x-1}P_{4-x}O_{12}$, crystallizes in the rhombohedral ($R\bar{3}m$) space group for the composition of $x < 2.8$ or $x > 3.2$ at room temperature, with Na occupying two distinct sites, namely Na1 and Na2 (Fig. 2) [63]. However, upon changing the Na-ion composition, i.e. $2.8 \leq x \leq 3.2$, or upon lowering the temperature, $Na_xZr_2Si_{x-1}P_{4-x}O_{12}$ undergoes a monoclinic transition, primarily into the $C2/c$ space group, due to Na-ion ordering in the framework breaking the degeneracy of the Na2 (Wyckoff position: 18e) and/or Na1 (6b) sites [63, 64]. In general, NaSICON compounds can be represented by the formula, $Na_xM_2(XO_4)_3$, where M is a 3*d* and/or 4*d* transition metal(s) and X is a high-valent non-redox-active cation such as P^{5+}, Si^{4+}, As^{5+}, Ge^{4+}, Mo^{6+}, and Nb^{5+} [65]. Thus, depending on the redox activity of the M cation and Na content within the framework, NaSICONs can act as either positive (cathode) or negative (anode) electrodes in a NIB.

The NaSICON unit cell consists of lantern units as shown in Fig. 2, built of MO_6 octahedra and XO_4 tetrahedra connected in a corner-shared fashion. Because of the isolated MO_6 octahedra, NaSICONs typically suffer from poor electronic conductivity [63]. Apart from Na1 and Na2, previous studies have reported the existence of a third Na site, namely Na3 (Wyckoff position 36f) [66]. However, such Na3 sites are transient sites (destabilized by electrostatic repulsions) and exhibit negligible Na occupancy at room temperature [66]. Among Na1 and Na2, the Na1 site typically is fully occupied at low Na concentrations (in $Na_xM_2(XO_4)_3$), while the Na2 sites are occupied only at higher Na content. Thus, during charging in NaSICON electrodes, Na is typically extracted from the Na2 site.

In terms of Na mobility, NaSICONs generally exhibit facile Na conduction, particularly around $x = 3$ in $Na_xM_2(XO_4)_3$, with the key migration being a Na atom hopping from a Na1 to an adjacent, vacant Na2 site (or vice-versa, see Fig. 2) [67]. Notably, Na migration events within NaSICON structures are typically highly correlated or follow a concerted mechanism, i.e., a Na hop from a Na1 to a Na2 site is typically dependent on its local environment and the other Na hops within the structure (see diffusion unit inset in Fig. 2). For example, a recent computational study employed DFT-NEB calculations in conjunction with a kinetic Monte Carlo model to statistically quantify the variations in "local" Na migration barriers on the overall Na conductivity and found a high degree of correlation among Na hops during their simulations [65]. Other reports

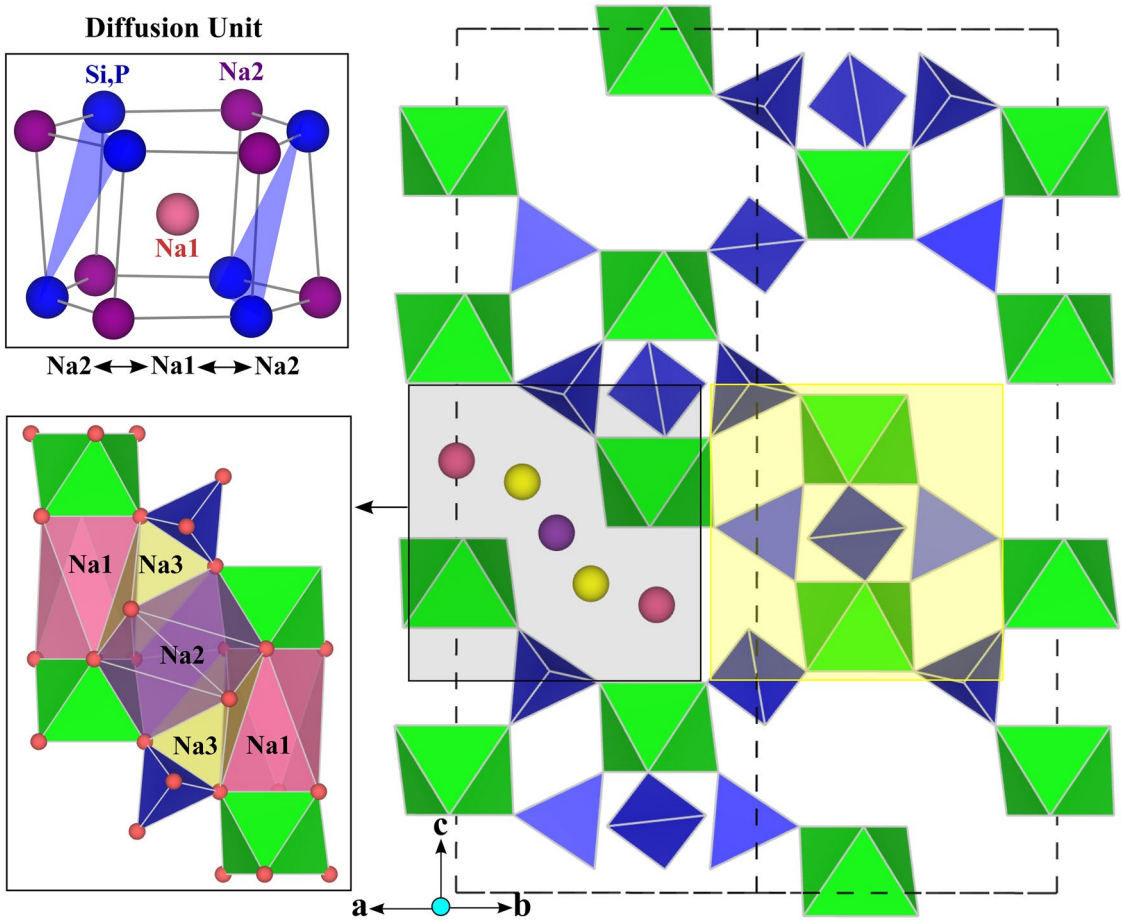

Figure 2: $R\bar{3}m$ conventional cell of a typical NaSICON is displayed in the right panel, with dashed black lines indicating the extent of the unit cell. Green, blue, pink, purple, and yellow spheres/polyhedra represent TM, Si/P, Na1, Na2, and Na3 atoms/sites, respectively. Oxygen atoms form the vertices of each polyhedra (not shown as spheres in the figure). The lantern unit that forms the fundamental building block of the NaSICON structure is highlighted by the yellow box. The bottom left panel highlights the "full" Na migration trajectory, from one Na1 to another equivalent Na1 site, via intermediate Na2 or Na3 sites. The top left panel highlights the diffusion (or migration) unit within NaSICON [65], which highlights the typical bottleneck sites (indicated by the blue triangles) that govern migration barriers for Na hops from Na1 to nearby Na2 sites. The Zr and O atoms are not indicated in the diffusion unit inset.

have also considered correlated jumps between Na sites, albeit with the involvement of the transient Na3 site [66], such as-Na1 → Na3 → Na2 → Na3 → Na1 and Na2 → Na3 → Na3 → Na2, associated with different transient sites. Interestingly, such correlation among Na hops contribute to overall higher Na-conductivities, across all three directions, than via uncorrelated Na hops [68].

Single-TM NaSICONs

Among NaSICONs containing a single redox-active TM, the rhombohedral-$Na_3V_2(PO_4)_3$ (NVP) is a well-studied composition [69]. Specifically, NVP shows a reversible two-phase Na (de) intercalation, $Na_3V_2(PO_4)_3 \leftrightarrow NaV_2(PO_4)_3$ at an average voltage of ~ 3.4 V vs. Na, where the $V^{4+/3+}$ couple is redox-active [Fig. 3(a)] [70]. Also, NVP can reversibly intercalate an additional Na, to form $Na_4V_2(PO_4)_3$, at ~ 1.6 V vs. Na, corresponding to $V^{3+/2+}$ redox [70], potentially functioning as an anode, highlighting the potential for constructing NIBs with NaSICONs as both anodes and cathodes. Indeed, such symmetric NIBs using NVP as both electrodes, separated by a conventional organic electrolyte, demonstrated an output voltage of 3.0 V, an appreciable energy density of 138 Wh kg^{-1}, with reasonable cycle life (84% capacity retained over 3000 cycles) and rate performance [at 40 mA g^{-1}, Fig. 3(b)] [71].

While NVP exhibits reasonable cycling behavior as a cathode (~ 2.7% capacity loss after 50 cycles at 1 C) [69], a number of attempts have been made to further improve the cycle life and, more importantly, the electronic conductivity, including doping with higher-valent cations (such as La [72], W [73], and Mo) [74], and creating unique nanosized cathode architectures with carbon coating [75–78]. For instance, hierarchical frameworks with carbon-coated nanosized NVP particles have been reported

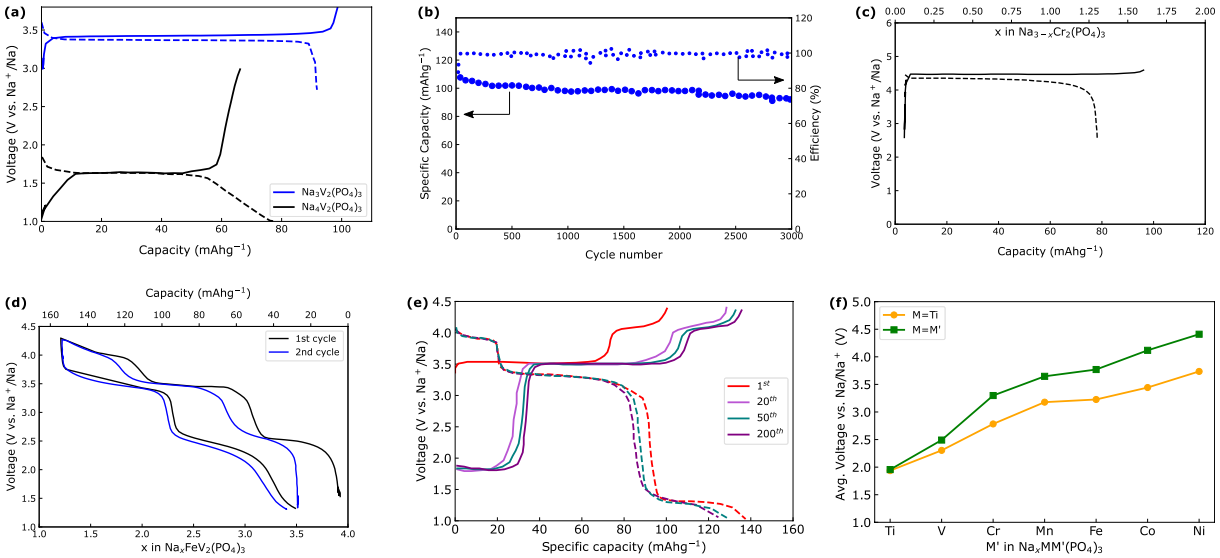

Figure 3: (a) Electrochemical voltage-capacity curves of NVP as cathode (blue lines) and NVP as anode (black lines). (b) Cycling behavior along with Coulombic efficiency of symmetric NVP cells, where NVP (with different Na contents) is used as both anode and cathode. (c) Electrochemical charge–discharge behavior in the high-voltage NCP NaSICON. (d) First and second electrochemical cycles in Fe-V mixed-TM cathode. (e) Charge–discharge cycling behavior in V-Cr mixed NaSICON. (f) DFT-calculated average Na intercalation voltages in single and mixed-TM (i.e., Ti^{+} another 3*d* metal) NaSICONs. Data from Refs. [70, 71, 79–81] and [63] was digitized and replotted in panels (a), (b), (c), (d), (e), and (f), respectively, with the corresponding copyrights with 2012 Elsevier B.V., 2018 American Chemical Society, 2018 American Chemical Society, 2021 American Chemical Society, 2020 WILEY–VCH Verlag GmbH & Co. KGaA, Weinheim, and 2021 Royal Society of Chemistry.

to exhibit significantly improved capacity retention (48% overall capacity fade at 20 C) over ~ 10,000 cycles [75]. Note that for Na-ion batteries to be cost-competitive with LIBs, TMs that are less expensive than V may have to be utilized.

Although NVP can be used as an anode, the $NaTi_2(PO_4)_3$ (NTP) is the typically preferred option since NTP exhibits reversible Na (de)intercalation forming $NaTi_2(PO_4)_3$ at 2.10 V vs. Na (thus higher capacity as anode), utilizing the $Ti^{4+/3+}$ redox pair [82]. However, symmetric cells with NTP as both electrodes delivered an underwhelming operating voltage of ~ 1.7 V, unlike NVP [83]. Other single-TM NaSICONs that have been studied experimentally include rhombohedral-$Na_3Cr_2(PO_4)_3$ (NCP) [79] and monoclinic-$Na_3Fe_2(PO_4)_3$ (NFP) [84]. Importantly, NCP is reported to exhibit a Na (de)intercalation voltage of ~ 4.5 V vs. Na, based on $Cr^{4+/3+}$ redox, which is perhaps the highest experimentally reported voltage among bulk single-TM NaSICON systems so far [Fig. 3(c)]. Single-TM NaSICONs based on Mn, Co, and Ni have not been studied experimentally, while a recent computational study indicated that Mn- and Co-based single-TM NaSICONs may be experimentally synthesizable [63].

Theoretically, NaSICON cathodes can exhibit a capacity of 117 mAh g^{-1} [69, 79] corresponding to the reversible intercalation of 2 Na per $Na_xM_2(XO_4)_3$ formula unit. Note that the final Na atom (i.e., $Na_1M_2(XO_4)_3$) has not been reversibly removed in electrochemical experiments so far in single-TM systems [85]. However, this theoretical capacity is still lower than what is practically exhibited by layered transition metal oxides [37], limiting the energy densities of NaSICON cathodes. Moreover, practical capacities achieved in experiments are typically lower than theoretical estimates, with NVP, NTP, NFP, and NCP delivering discharge capacities of ~ 93 mAh g^{-1} (at 0.05 C-rate) [70], ~ 120 mAh g^{-1} (at 2.0 mA cm^{-2}) [86], 61 mAh g^{-1} (at 0.2 C) [84] and 79 mAh g^{-1} (at 0.5 C) [79], respectively. Also, the poor intrinsic electronic conductivity in NaSICONs does cause significant hysteresis during electrochemical cycling, leading to less-than-desired rate performance. While nanosizing and coating strategies have been explored to address the electronic conductivity issue [72–78], studies have also explored mixed-TM NaSICONs to improve practical energy densities (see mixed-TM section below).

Another strategy to enhance the electrochemical voltages of NaSICON frameworks is to use sulfate moieties (instead of phosphates), since S^{6+} exerts a stronger inductive effect on the surrounding O^{2-}, enhancing the ionic character of the TM–O bonds, which in turn results in higher voltages. Indeed, theoretical calculations indicate a higher intercalation voltage for $Fe^{3+/2+}$ redox in sulfate NaSICON (~ 3.2 V) [87], compared to the voltage for $Fe^{3+/2+}$ redox in a phosphate NaSICON (~ 2.6 V) [63]. However, a complete substitution of P with S causes a steep reduction in the theoretical capacity, since the number of extractable Na goes down from 4 per formula unit in phosphates ($x = 0$ to in $Na_xM_2(PO_4)_3$) to 2 per formula unit in sulfates ($x = 0$ to 2 in $Na_xM_2(SO_4)_3$). Moreover, recent calculations

in $Na_xFe_2(SO_4)_3$ [87], indicate a higher migration barrier for Na1–Na1 hop (0.89 eV) compared to $Na_xFe_2(PO_4)_3$ (0.31 eV) at $x \sim 0$. Additionally, at certain Na compositions, sulfate NaSICONs may be competing thermodynamically with the alluaudite structure (see "Alluaudites" section) to physically exist. Thus, a complete substitution of phosphates with other polyanion moieties may not entirely be beneficial in improving the electrochemical performance of NaSICONs, but partial substitution of P with S, Si, etc., may enhance the performance marginally.

Mixed-TM NaSICONs

To improve the electrochemical performance of NVP, previous studies have attempted adding other redox-active TMs, including Ti, Cr, Mn, Fe, Co, Ni, and Cu, creating mixed-TM NaSICONs [77, 81, 88–91]. For example, partial substitution of V with Fe [Fig. 3(d)] allows the extraction of 2.76 Na^+ per NaSICON formula unit (versus two Na per NVP formula unit), resulting in increased capacity (153 mAh g^{-1} vs. 93 mAh g^{-1} for NVP) and a higher average voltage due to the $V^{5+/4+}$ redox couple (3.9 V vs. 3.4 V for NVP) [80]. Similarly, introducing Cr also activates $V^{5+/4+}$ redox (in $Na_xV_{1.5}Cr_{0.5}(PO_4)_3$), resulting in an appreciable increase in both the average voltage (~4.1 V) and capacity (~150 mAh g^{-1} at 30 mA g^{-1}) versus NVP [Fig. 3(e)] [81]. While Ni addition to NVP does not result in any capacity improvement (67 mAh g^{-1} at 5 C over 500 cycles) [89], Mn infusion in NVP improves cycling stability at high rates (~20 C) [88]. The V-Ti mixed NaSICON does not activate the $V^{5+/4+}$ redox couple, but exhibits stable phases at $x = 1$, 2, 3, and 4 (x in $Na_xTiV(PO_4)_3$), all of which can be prepared electrochemically or via solid-state reactions. The electrochemical reduction of $NaTiV(PO_4)_3$ to $Na_4TiV(PO_4)_3$ follows several single and two-phase regions, involving both $V^{4+/3+/2+}$ and $Ti^{4+/3+}$ redox couples, at an overall average voltage of ~2.36 V vs. Na [92].

Apart from V-based mixed-TM NaSICONs, studies have explored Mn-based mixed-TM frameworks as well [93, 94]. For example, Zhang et al. [93] synthesized $Na_4MnCr(PO_4)_3$ and observed an appreciably high energy density, upon Na removal, of 566.5 Wh kg^{-1}, a capacity of ~160 mAh g^{-1} at 0.05 C, and an average voltage of ~3.53 V vs. Na that involves $Mn^{4+/3+/2+}$ and $Cr^{4+/3+}$ redox couples. In the case of Mn–Ti mixed NaSICON, the framework exhibits multiple voltage plateaus when discharged between 1.5 and 4.2 V vs. Na, namely, 4 V (corresponding to $Mn^{4+/3+}$), 3.5 V ($Mn^{3+/2+}$) and 2.1 V ($Ti^{4+/3+}$), corresponding to the exchange of 3 Na atoms, and delivers a capacity of 139 mAh g^{-1} against a carbon anode at 0.5 C [94]. However, the voltage plateau at ~2.1 V does cause significant hysteresis between charging and discharging, which can be suppressed via synthesis of non-stoichiometric mixed NaSICONs that suppresses the $Ti^{4+/3+}$ redox [95]. Notably, the Jahn–Teller distortion of Mn^{3+} is significantly suppressed by the presence of other TMs, such as Ti, V or Cr, in the mixed NaSICONs [89, 93, 94].

While only a handful of mixed-TM NaSICONs have been successfully synthesized experimentally, a recent computational study examined possible single and mixed-TM compositions across the 3*d* series [63]. Specifically, Singh et al. calculated the average intercalation voltage, capacity, and pseudo-binary formation energies of 28 different $Na_xMM'(PO_4)_3$ compositions, where M and M′ can be Ti, V, Cr, Mn, Fe, Co, or Ni, with an emphasis on qualitative trends in Ti-based mixed NaSICONs [Fig. 3(f)] [63]. Apart from identifying Co- and Ni-based NaSICONs to exhibit high theoretical voltages, the study reported that the qualitative trends in voltages across the 3*d* series followed the standard reduction potentials of the TMs undergoing redox. Additionally, Singh et al. highlighted that the voltage plateau for a given TM redox (e.g., $V^{4+/3+}$) occurred at similar values in both single-TM ($Na_xV_2(PO_4)_3$) and mixed-TM ($Na_xVM'(PO_4)_3$) systems. Also, the authors reported that Mn- and Co-based NaSICONs may be experimentally synthesizable, highlighting the important contributions and guidance theoretical studies can provide in this vast chemical space [63].

Overall, NaSICONs form a promising and robust class of polyanionic intercalation frameworks that can act as cathodes and enhance the development and performance of NIBs. The experimental and theoretical studies so far have sampled only a small sub-space of the diverse chemical space that can potentially form NaSICON compounds, thus providing several different handles to tune electrochemical performance. For example, moving from single-TM NaSICONs to mixed-TM structures have been shown to enhance both the reversible Na capacity and the average intercalation voltage in several systems [57, 78, 81, 86]. Similarly, doping/substituting the anionic framework, via replacing P with other non-redox-active cations like Si, S, etc. [87, 96], is another handle to tune electrochemical performance as well. Recent studies have also increased the understanding of the thermodynamic phase behavior [63, 97], including specific Na-orderings that NaSICON frameworks can exhibit, as highlighted by the recent discovery of the $Na_2V_2(PO_4)_3$ as a stable phase [80]. Nevertheless, the low theoretical (and practical) capacities and the poor intrinsic electronic conductivity does form major bottlenecks for NaSICONs to overcome in order to be used as NIB cathodes in a more widespread manner, where novel coating techniques and cathode hierarchy designs can help in optimizing the electron transport.

Olivines and ortho-polyanions

Another popular polyanionic framework that has been explored for NIBs, particularly because of its high theoretical capacity (~154 mAh g^{-1}), is the olivine, which is inspired by their

commercially successful Li analog, $LiFePO_4$ [98, 99]. Olivines exhibit a general formula of A_xMXO_4, where A is the intercalant (Li, Na), M is a redox-active 3*d* TM (usually Fe, Mn, or Ni) and X is a high-valent non-redox-active cation (usually P^{5+}, but Si^{4+} is also known) [99–102]. The olivine structure consists of MO_6 octahedra that share edges and corners with XO_4 tetrahedral units, with A atoms forming a one-dimensional "tunnel" along the *b*-axis [Fig. 4(a)]. Thus, olivines are 1D conductors of intercalant ions, unlike NaSICONs which conduct ions in 3D. Indeed, a theoretical study reported a Na migration barrier of 0.21–0.43 eV along the *b*-axis in $NaFePO_4$, which indicates facile movement of Na along the 1D tunnels [103, 104]. Another theoretical study also reported an analogous barrier of ~ 280 meV [Fig. 4(b)] for Na migration $FePO_4$, with an increase in barrier up to ~ 375 meV for vacancy migration in $NaFePO_4$, along the *b*-axis [104].

Similar to NaSICONs, olivines usually exhibit poor electronic conductivity [105, 106], with doping (e.g., introducing Mg^{2+} instead of Mn in $NaMnPO_4$) [107, 108], nanosizing and coating techniques often used to improve their electronic transport and eventual rate performance [109]. Na-olivines are usually synthesized from their Li analogs (e.g., $LiFePO_4$) via ion exchange [99] since alternate synthesis routes (e.g., solid-state synthesis at high temperature and pressure) typically produce the thermodynamically stable maricite polymorph, which is electrochemically inactive [103]. The maricite structure, which has an identical composition and space group (*Pmna*) to the olivine, involves a complete exchange of sites between A and M atoms, rendering no feasible channels for long-range A diffusion in the structure, resulting in their inactivity in electrochemical setups. However, recent studies have claimed that 2D Na diffusion is feasible in nanosized maricite-$NaFePO_4$ [110], particularly with amorphization of $FePO_4$ [111], which requires further examination.

In terms of the thermodynamic phase behavior of Na (de) intercalation in olivines, a previous study by Saurel et al. has claimed that during charging, $NaFePO_4$ exhibits a single phase till $Na_{2/3}FePO_4$, beyond which a two-phase region exists [112], which is different from the phase behavior observed in the Li analog [113]. Theoretical calculations are partly in agreement with experiments in predicting $Na_{2/3}FePO_4$ and $Na_{5/6}FePO_4$ to be stable [Fig. 5(a)] [114]; but galvanostatic intermittent titration technique (GITT) measurements did not indicate the presence of $Na_{5/6}FePO_4$ [114]. Apart from specifying that the phase behavior of $NaFePO_4$ undergoes changes with rate of Na deintercalation, Saurel et al. also concluded that during discharge of desodiated Na_xFePO_4, the system exhibited two concomitant two-phase regions (consisting of olivine frameworks with different Na content) that appeared like a three-phase mixture at low rates, accompanied by significantly large strains [112]. While the co-existence of three phases is not possible at a given temperature and pressure in a pseudo-binary system, such as Na_xFePO_4, the reported mechanical strains is likely caused by other side reactions. Hence, more theoretical and computational work is required to fully understand the phase behavior of $NaFePO_4$ and other Na-based olivines.

Electrochemically, olivine-$NaFePO_4$ exhibits ~ 80% of its theoretical capacity (i.e., 125 mAh g^{-1} experimentally versus theoretical 154 mAh g^{-1}) over 50 cycles at an average voltage of ~ 2.7 V vs. Na and 0.05 C-rate [115]. Thus, in terms of eventual electrochemical output, olivines are quite similar to single-TM NaSICONs, with marginally higher capacity at lower voltages. An amorphous version of $FePO_4$, obtained via complete desodiation of $NaFePO_4$, has also been reportedly explored as a cathode material, but with similar electrochemical performance compared to a crystalline, nanosized olivine framework [111, 116]. Apart from the Fe-olivine, $NaMnPO_4$ has been experimentally synthesized [117] and electrochemically tested as a cathode [100], with the structure exhibiting significant capacity fading [from ~ 150 mAh g^{-1} in first cycle to ~ 85 mAh g^{-1} in the 20th cycle at C/50, see Fig. 5(b)] [100]. While the Co analog ($NaCoPO_4$) exhibits a different structure compared to

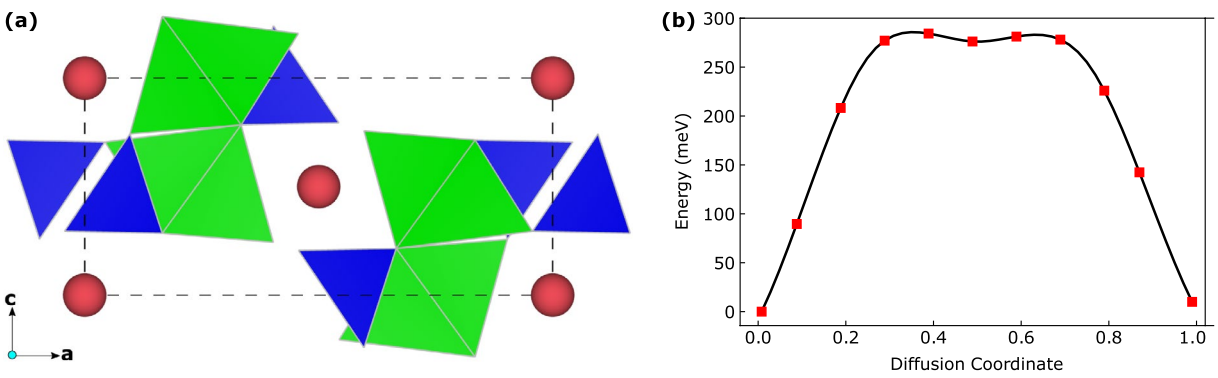

Figure 4: (a) Conventional cell of olivine, with green, blue, and pink polyhedra/spheres indicating TM, P, and intercalant sites. (b) DFT-NEB calculated barrier for Na migration along *b*-axis in $FePO_4$. Data replotted from Ref. [104], copyright 2011 Royal Society of Chemistry.

the olivine [118], the Ni analog has been explored mostly as a supercapacitor instead of a battery cathode [101, 119].

An extension of the olivine composition is the orthorhombic (space group: *Pn*) A_2MXO_4 framework, also referred to as orthosilicates (X = Si) or orthophosphates (X = P), which has been explored as cathodes in both NIBs and LIBs [120–123]. Notably, ortho-polyanion frameworks can exhibit high theoretical capacities (~ 270 mAh g^{-1}) [124] corresponding to the extraction of two Na ions per formula unit, with facile Na diffusion (calculated migration barrier of ~ 0.26 eV in Na_2MnSiO_4) [125]. A high fraction (~ 97%) of the theoretical capacity in ortho-polyanionic frameworks can be obtained electrochemically, as indicated by Na_2MnSiO_4, which exhibited an initial charging capacity of ~ 261 mAh g^{-1} at 0.1 C in the voltage window of 1.5–4.5 V vs. Na [124]. However, subsequent electrochemical discharge of $MnSiO_4$ yielded a lower capacity of ~ 182 mAh g^{-1} (corresponding to intercalation of ~ 1.3 Na per $MnSiO_4$). Thus, irreversible electrolyte decomposition is likely to have contributed significantly during the first charge [124].

Capacity degradation after first charge, similar to Na_2MnSiO_4, was also observed in Na_2FeSiO_4, where only ~ 0.9 Na could be intercalated after a first charge that supposedly extracted ~ 1.9 Na from the structure [102]. On the other hand, Na_2CoSiO_4 exhibited lower polarization during electrochemical discharge/charge compared to the Mn and Fe analogs, with a capacity of 125 mAh g^{-1} at 0.05 C, but the material exhibits several phase transitions during Na (de)intercalation [126]. Although experimental studies have attributed the capacity degradation in Fe and Mn orthosilicates to electrolyte decomposition [121, 125], theoretical studies indicate that the Na_2MnSiO_4 becomes unstable (with oxygen release) beyond 75% Na extraction [125], which can also contribute to capacity degradation. Nevertheless, there are also reports of capacity retention improvements in both Na_2FeSiO_4 and Na_2MnSiO_4 upon adding select electrolyte additives [102, 124, 127].

In terms of orthophosphates, a recent work by Lu et al. [123] reported the synthesis of a novel $Na_{0.6}Fe_{1.2}PO_4$ orthophosphate compound but with low capacity (85 mAh g^{-1} initial capacity at C/20 that degrades to ~ 70 mAh g^{-1} after 50 cycles) at an average voltage of ~ 3.0 V vs. Na. Another class of orthophosphates that has been explored as Na cathodes is $NaVOPO_4$, which can crystallize in several different polymorphs based on synthesis techniques [128–134]. Although previous experimental and theoretical studies have focused on the thermodynamically stable-α, the β, and the layered-α_I polymorphs [135–138], proton intercalation is known to contribute to the observed electrochemical response [136]. The origin of protons within the $VOPO_4$ structure is unclear but is often attributed to the reagents that are used to chemically delithiate $LiVOPO_4$, which in turn forms the base cathode framework for subsequent sodiation [136]. Hence, more detailed investigations are required to fully decouple the role of proton (de)intercalation within $VOPO_4$ frameworks and better understand the electrochemical activity of Na within the $VOPO_4$ polymorphs.

In summary, olivines and ortho-polyanionic frameworks often appear promising as Na cathodes giving their high theoretical capacities among polyanionic cathodes in Na-ion systems and the robust electrochemical performance observed in corresponding Li-ion analogs. However, experimental evidence in Na-containing olivines is quite mixed, with the thermodynamic instability of the olivine framework often leading to amorphization. This is not to say that amorphization of electrode frameworks intrinsically leads to poorer electrochemical performance, but it is typically difficult to improve performance in a systematic manner. Structural transitions may play a role in the capacity degradation observed in orthosilicates, although more

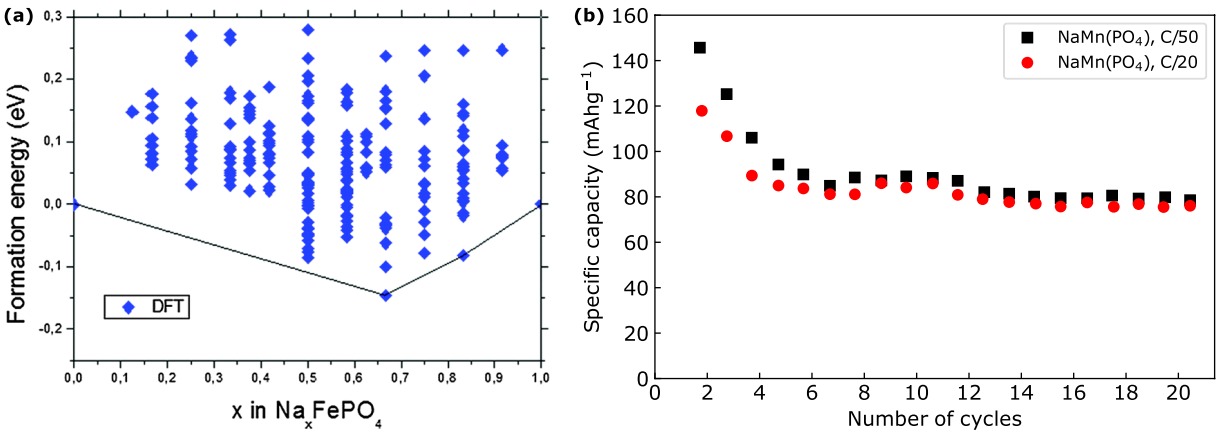

Figure 5: (a) DFT-calculated 0 K phase diagram (or convex hull) of Na exchange in pseudo-binary Na_xFePO_4 system. The set of DFT-predicted stable compositions are indicated by the solid black lines. Figure reproduced from Ref. [114], copyright 2016 Royal Society of Chemistry. (b) Electrochemical cycling behavior, as quantified by capacity obtained versus number of charge–discharge cycles in $NaMnPO_4$ at C/50 (black squares) and C/20 (red circles) rates. Data digitized and replotted from Ref. [100], copyright 2015 Royal Society of Chemistry.

experimental and computational investigations are required to ascertain the origin of such degradation. Finally, decoupling proton and Na (de)intercalation effects is imperative to accurately quantify and compare the performance of $VOPO_4$ frameworks against other polyanionic frameworks. In summary, polyanionic frameworks other than olivines and ortho-polyanions are likely more pertinent for improving the energy densities and electrochemical performance of NIBs.

Alluaudites

Alluaudites are primarily phosphate-based minerals with a rigid "open" framework [139] that is suitable for Na (or large alkali) ion intercalation. Alluaudites, with the monoclinic $C2/c$ space group, exhibit a composition of [A(2)A(2)′][A(1)A(1)′A(1)″] $M(1)M(2)_2(PO_4)_3$, following the terminology of Leroux and Hatert, where A sites host Na and M sites signify TMs [140, 141]. The symmetrically distinct A and M sites are distinguished by numbers and primes (' or ″), with all A sites typically exhibiting partial Na occupancy resulting in a simplified composition of the form $A(2)A(1)M(1)M(2)_2(PO_4)_3$. The M(1) and M(2) metal ions form distorted $M(1)O_6$ octahedra and $M(2)_2O_{10}$ dimers, respectively, which share edges to form zigzag chains [Fig. 6(a)] along the *b*-axis. The PO_4 tetrahedra bridge pairs of M–O zigzag chains via corner-sharing [Fig. 6(a)], which result in two 1D Na migration pathways along the *c*-axis, namely, corner tunnel 1 (A(1) sites) and edge-centered tunnel 2 (A(2) sites). Sulfate-based alluaudites also exist with associated changes in the structure and composition. For example, the M(1) sites are occupied by Na in sulfate alluaudites [Fig. 6(b)] causing a change in the general composition to $AA'BM(2)_2(SO_4)_3$ [142], where A and A′ are identical to A(1) and A(2) sites, respectively, of phosphate alluaudites (with partial Na occupancy on both sites) and B is the same as the M(1) site with full Na occupancy. Thus, sulfate alluaudites typically contain one distinct TM compared to the two distinct TMs in phosphate alluaudites.

$Na_xMnFe_2(PO_4)_3$ was the first alluaudite to be investigated for its Na electrochemical properties [143], with a theoretical capacity of ~ 109 mAh g^{-1}, assuming two moles of Na to be reversibly extracted per formula unit. Practically, only one Na per formula unit can be reversibly (de)intercalated from the structure, corresponding to a capacity of ~ 50 mAh g^{-1} across a voltage window of 1.5–4.3 V vs. Na, with marginal capacity improvements upon reduction in cathode particle size [Fig. 7(a)] [143, 144]. The feasible (de)intercalation of only one Na per formula unit is attributed to higher migration barriers (~ 1.28 eV) for Na hops across A(1) sites compared to A(2) sites (~ 0.31 eV), as computed by BVSE calculations [144]. Note that it is $Fe^{3+/2+}$ redox couple, not $Mn^{3+/2+}$ that is redox-active upon Na (de) intercalation in $Na_xMnFe_2(PO_4)_3$ [144]. $Na_2VFe_2(PO_4)_3$ shows marginally better performance to that of $Na_xMnFe_2(PO_4)_3$, with a capacity of ~ 67 mAh g^{-1} (corresponding to 1.24 mol of Na exchange) over a 1.5–4.5 V (vs. Na) window at 5 mA g^{-1} [145]. Unlike Mn–Fe alluaudite, the authors claimed that both V and Fe are redox-active in the V–Fe alluaudite, based on their cyclic voltammogram data [145], but this requires further verification.

Other phosphate alluaudites reported, namely Co–Fe ($Na_2Co_2Fe(PO_4)_3$) [146], Ni–Fe ($Na_2Ni_2Fe(PO_4)_3$) [147, 148] and Co–Cr (i.e. $Na_2Co_2Cr(PO_4)_3$) [149], showed instances of conversion reactions (including formation of metallic Fe and Co), electrolyte decomposition against Na metal electrode, and/or poor electrochemical performance. Non-Na-stoichiometric, single-TM phosphate alluaudites have also been explored as cathodes. For example, $Na_{1.47}Fe_3(PO_4)_3$ [150] and $Na_{1.86}Fe_3(PO_4)_3$ [151] compounds exhibited similar voltages (~ 3 V vs. Na) and capacities (~ 80 mAh g^{-1}) upon Na discharge, after a first charge to remove part of the existing Na. Overall, phosphate alluaudites seem to exhibit poor electrochemical capacity (~ 50–80 mAh g^{-1}) [143, 144] at a reasonable average voltage (~ 2.8–3 V vs. Na) [143, 144, 150, 151].

Sulfate alluaudites exhibit better electrochemical performance than the phosphate analogs, largely driven by higher voltages due to the stronger inductive effect of S^{6+} compared to P^{5+} [152]. For example, $Na_2Fe_2(SO_4)_3$ exhibits an average voltage of 3.8 V vs. Na, the highest reported for $Fe^{3+/2+}$ redox couple so far, with a smoothly sloped voltage profile over a reversible capacity of 102 mAh g^{-1} (~ 85% of the theoretical capacity of ~ 120 mAh g^{-1}, corresponding to 2 Na exchange) for 30 cycles at 0.05 C [Fig. 7(b)] [142]. Subsequent DFT calculations predicted average voltages of ~ 4.40, 5.15, and 5.25 V for full desodiation of Mn, Co, and Ni sulfate alluaudites (i.e., $Na_2M_2(SO_4) \leftrightarrow M_2(SO_4)_3$), respectively [153]. Similar DFT calculations on alluaudites with Na-excess compositions also predicted high voltages. For example, DFT calculations in $Na_{2.5}Co_{1.75}(SO_4)_3$ (mimicking the experimentally synthesized composition of $Na_{2.32}Co_{1.84}(SO_4)_3$) and $Na_2Mn_2(SO_4)_3$ (mimicking $Na_{2.44}Mn_{1.79}(SO_4)_3$) predicted average voltages of ~ 4.98 V (for full desodiation) and ~ 4.4 V (for half desodiation) vs. Na, respectively [154, 155]. However, neither Na-excess composition displayed appreciable electrochemical activity with conventional Na-liquid electrolytes, indicating the need for developing electrolytes that have better anodic stability.

Despite the better electrochemical properties, sulfate alluaudites are prone to thermal and moisture degradation due to the presence of SO_4^{2-} moieties [156]. That apart, a careful choice of protocols is necessary (e.g., ionothermal vs. solid-state reaction) to ensure that impurities or unreacted precursors are not left behind during synthesis of sulfate alluaudites [142, 157]. Appropriate choice of synthesis procedures, i.e., using ionothermal-based methods, have shown improvements in capacity retention (> 90%) and the capacity itself (≥ 100 mAh g^{-1}) [157]. However, ionothermal synthesis can also result in non-stoichiometric alluaudites (e.g.,

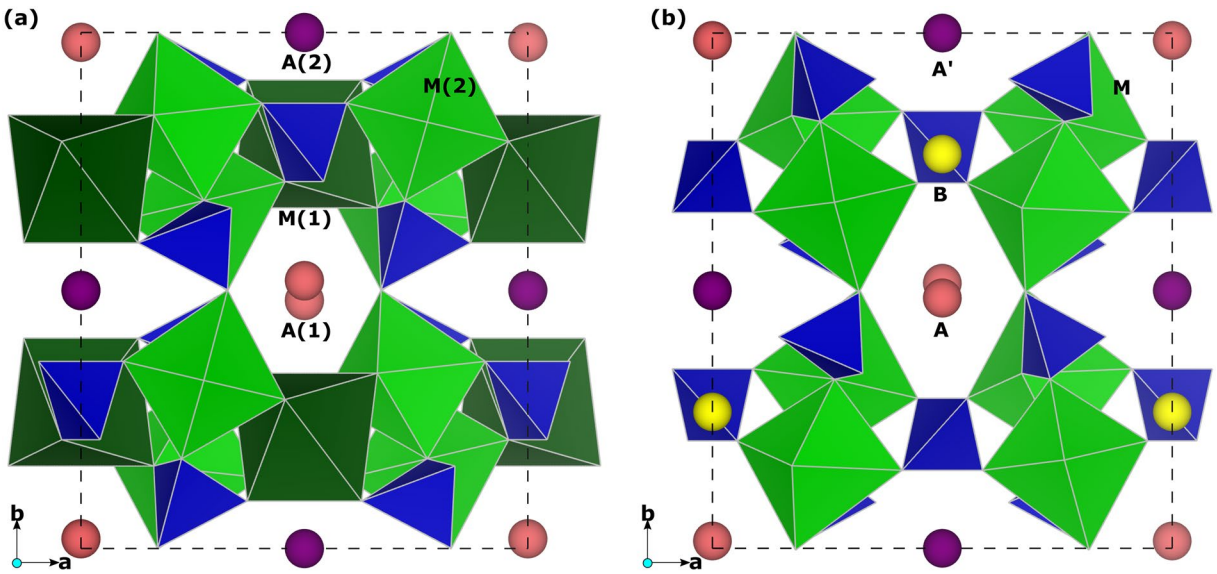

Figure 6: Conventional cell of (a) phosphate and (b) sulfate alluaudite. Pink, purple, and yellow spheres indicate Na sites, namely A(1) and A(2) sites in phosphate, and A and B sites in sulfate alluaudite. Green and blue polyhedra indicate TMO_6 and XO_4 groups, respectively (X = P or S). Dark and light green polyhedra in panel (a) signify the M(1) and M(2) sites in the phosphate alluaudite. Note that the M(1) site in panel (a) is identical to the B site in panel (b). Dashed black lines in both panels highlight the boundaries of the unit cell.

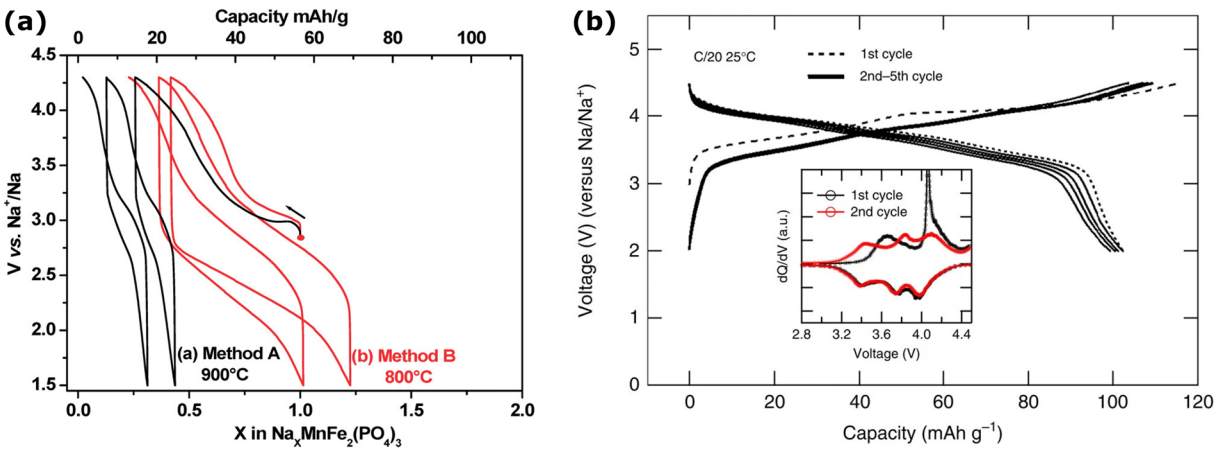

Figure 7: (a) Electrochemical voltage-capacity evolution upon charge and discharge of $Na_xMnFe_2(PO_4)_3$, synthesized using two different protocols (as highlighted by red and black lines). Figure reproduced from Ref. [143], copyright 2010 American Chemical Society. (b) Voltage–capacity curves, from 1st to 5th electrochemical cycle, in $Na_xFe_2(SO_4)_3$, with the inset displaying the differential capacity against voltage for the first 2 cycles. Figure reproduced from Ref. [142], copyright 2014 Springer Nature.

$Na_{2.4}Fe_{1.8}(SO_4)_3$ vs. $Na_2Fe_2(SO_4)_3$) [157], with the non-stoichiometric composition often exhibiting lower capacity compared to the corresponding stoichiometric version [158–161]. Additionally, at certain Na compositions, sulfate alluaudites can compete with sulfate NaSICONs (see "NaSICONs" section) in terms of thermodynamic stability, which can influence the choice of synthesis protocols as well as electrochemical performance. For example, alluaudite-$Na_2Fe_2(SO_4)_3$ is more stable than NaSICON-$Na_2Fe_2(SO_4)_3$, which results in higher average voltage (3.8 V vs. ~ 3 V) and the presence of low migration barrier diffusion pathways (~ 0.3–0.5 eV vs. ~ 0.89 eV) in the alluaudite structure [87]. Also, mixed-TM sulfate alluaudites have also been explored as Na cathodes, as indicated by studies on Fe–Mn and Co–Mn frameworks [162, 163], but with lower capacities compared to single-TM compositions (largely attributed to electrochemical inactivity of Mn^{2+}). Overall, sulfate alluaudites are more promising than phosphate alluaudites in terms of electrochemical performance, but the high voltages required for electrochemical operation and the sensitivity of the framework to moisture exposure and synthesis protocols make it difficult to be used in practical NIBs.

Pyrophosphates

Pyrophosphates exhibit better thermal stability and resistance to oxygen evolution and moisture exposure compared to other polyanionic frameworks because they are typically synthesized above 550 °C by thermal decomposition of phosphates (via steam release and the formation of bridging –P–O–P– bonds) [164, 165]. An example chemical reaction that yields $Na_2FeP_2O_7$ via solid-state synthesis can be written as follows [165],

$$Na_2CO_3 + 2(NH_4)_2HPO_4 + FeC_2O_4 \cdot 2H_2O \rightarrow Na_2FeP_2O_7 + 4H_2 + 2N_2 + 3CO + 7H_2O$$

To date, Fe-, Mn-, and Co-based pyrophosphates have been explored as Na intercalation cathodes, with the pyrophosphates crystallizing in different polymorphic forms depending on the 3*d* TM. For example, Fe-pyrophosphate ($Na_2FeP_2O_7$), and Mn-pyrophosphate ($Na_2MnP_2O_7$) can exhibit the $P1$ or $P\bar{1}$ space groups belonging to the triclinic crystal system, while Co-pyrophosphates can be in one of four distinct polymorphs, namely, tetragonal ($P4_2/mnm$), orthorhombic ($Pna2_1$), and triclinic ($P\bar{1}$) at the $Na_2CoP_2O_7$ composition [166, 167] and triclinic ($P1$) at $Na_{3.12}Co_{2.44}(P_2O_7)_2$ [168].

Both $P1$ and $P\bar{1}$ polymorphs of $Na_2FeP_2O_7$ have FeO_6 octahedra, sharing corner to form Fe_2O_{11} dimers. Two such dimers are interconnected by pyrophosphate (P_2O_7) units in a staggered fashion with both corner and edge sharing [Fig. 8(a)]. In the $P\bar{1}$ structure, there are six distinct crystallographic sites for Na ions, with the Na1, Na2 and Na3 exhibiting full Na occupancy and Na4, Na5 and Na6 sites displaying partial occupancy. Importantly, the calculated Na migration barriers in all three directions are similar (0.33–0.5 eV) [169], suggesting robust 3D Na conductivity in the structure. During electrochemical charging, $P\bar{1}$ maintains its structural framework, facilitating topotactic Na removal resulting in the formation of $NaFeP_2O_7$ [164]. Upon cycling [Fig. 8(b)], the $P\bar{1}$ structure exhibits a voltage of ~ 3 V vs. Na with a capacity of ~ 82 mAh g^{-1}, which is ~ 82% of the theoretical capacity, over 30 cycles at 0.l C [170]. Also, with partial substitution of Mn, $P\bar{1}$ $Na_2Fe_{0.5}Mn_{0.5}P_2O_7$ mitigates capacity fading that is typically observed in $Na_2FeP_2O_7$, with retention of ~ 84% of the initial capacity over 90 cycles [171]. Note that $NaFeP_2O_7$ undergoes a polymorphic transition upon heating (above 560 °C) to a monoclinic ($P2_1/c$) phase [170].

Unlike $P\bar{1}$, $P1$-$Na_2FeP_2O_7$ contains tetrahedral (Na1) and pyramidal (Na2) sites that each share two corners and edges with neighboring FeO_6 octahedra [165]. Additionally, Na migration in $P1$ happens in a 1D pathway, along the [011] direction [165]. Electrochemically, $P1$-$Na_2FeP_2O_7$ phase exhibits similar capacity (~ 90 mAh g^{-1}) as the $P\bar{1}$ structure in the voltage range of 2.0–4.5 V vs. Na, with four two-phase regions corresponding to 2.52, 2.99, 3.08, and 3.24 V, where DFT calculations have suggested that the extraction of Na at 2.52 V (during charging) is from the Na1 site [165].

The $P1$ and $P\bar{1}$ space groups of $Na_2MnP_2O_7$ are referred to as the β and layered polymorphs, respectively, and are different structures compared to $Na_2FeP_2O_7$ [172, 173]. The layered polymorph undergoes a polymorphic transition to the β phase at temperatures higher than 600 °C and does not show any significant electrochemical activity [173]. The β polymorph is built with Mn_2O_{11} dimers of corner-shared, distorted MnO_6 octahedra, which are bridged by P_2O_7, and exhibits 3D diffusion of Na (similar to $P\bar{1}$ $Na_2FeP_2O_7$) [172]. Experimentally, β-$Na_2MnP_2O_7$ displays a capacity of 80 mAh g^{-1} at 0.05 C at an average voltage of 3.6 V vs. Na [172], with marginal improvements in capacity with surface modification [174].

Thermodynamically, the stable polymorph of $Na_2CoP_2O_7$ is orthorhombic ($Pna2_1$), which exhibits a capacity of 80 mAh g^{-1} over an average voltage of 3 V for the $Co^{3+/2+}$ redox couple at 0.05 C [167]. The voltage-capacity profile displayed by the orthorhombic polymorph is smoothly sloped but the structure suffers from capacity fading beyond 20 cycles [167]. The metastable triclinic polymorph of $Na_xCoP_2O_7$ can be accessed by synthesizing the $x = 0.4$ composition. Subsequent electrochemical measurements with the triclinic polymorph exhibited a superior voltage (4.3 V vs. Na) than the stable orthorhombic polymorph with similar capacity (~ 80 mAh g^{-1}) but at higher rates (0.2 C) [175, 176]. Given that conventional Na electrolytes tend to exhibit irreversible decomposition at high voltages (> 4 V vs. Na) [175], the contribution of Na exchange to the capacity exhibit by the triclinic polymorph requires further investigation.

Pyrophosphates with excess Na content, particularly based on Mn and Fe have been explored with reasonable electrochemical performance [177, 178]. For instance, triclinic-$Na_{3.12}Mn_{2.44}(P_2O_7)_2$ displays a reversible capacity of 114 mAh g^{-1} at 0.1 C and 75% capacity retention after 500 cycles at 5 C [177]. Meanwhile, $Cr_2P_2O_7$ and TiP_2O_7 were cycled against Na between 0 and 3 V, with $Cr_2P_2O_7$ displaying potential to be used as an anode with an OCV ~ 2 V (238 mAh g^{-1} at 0.05 A g^{-1}; 194 mAh g^{-1} after 300 cycles at 0.1 A g^{-1} [179, 180].

Overall, the pyrophosphate class of compounds, despite exhibiting better structural stability than other polyanionic frameworks, displays similar or lower capacities (compared to other polyanions). Additionally, pyrophosphates have lower chemical flexibility to increase the average voltages and/or theoretical capacities, signifying the challenges in using such compounds as cathodes. However, more experimental and theoretical work is still required to understand the fundamental phase behavior and Na diffusion kinetics more robustly within this class of materials and to further improve their electrochemical performance.

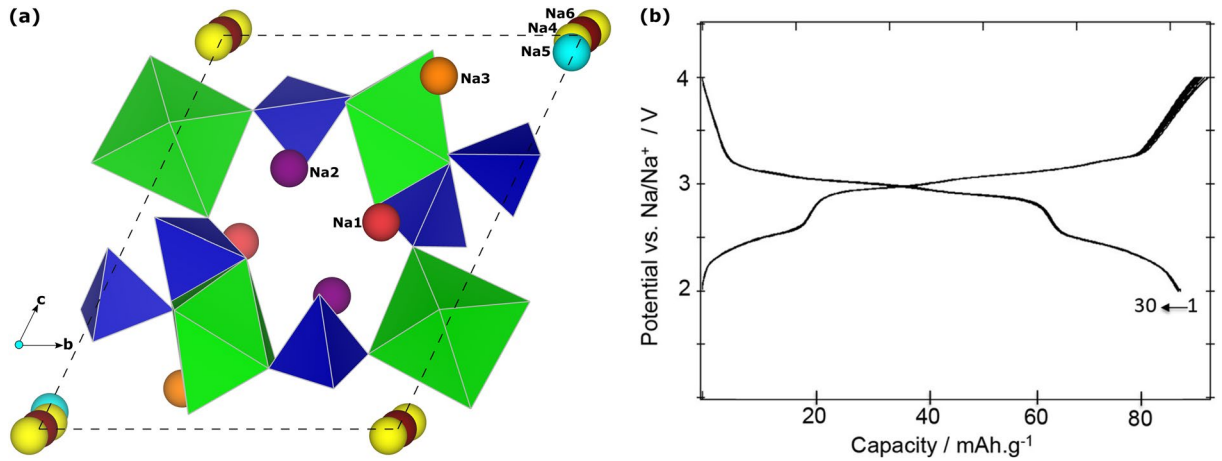

Figure 8: (a) Conventional cell of $P\bar{1}$ $Na_2FeP_2O_7$ pyrophosphate, with the pink, purple, orange, yellow, blue, and brown spheres signifying Na1, Na2, Na3, Na4, Na5, and Na6 sites, respectively. Green and blue polyhedra indicate TMO_6 and PO_4 groups, respectively. Dashed black line highlights the boundaries of the conventional cell. (b) Voltage-capacity profiles over the first 30 electrochemical cycles in $P\bar{1}$ $Na_xFeP_2O_7$. Figure reproduced from Ref. [164], copyright 2012 Elsevier B.V.

Fluoro-polyanions

The addition of fluorine as an anion, within oxide-based polyanionic frameworks, can elevate the intercalation voltage due to the stronger inductive effect exerted by F^- than O^{2-} [181]. Specifically, F^- reduces the electron density around TM cations and induces more ionicity in the TM-anion bonds, compared to O^{2-}, which results in higher voltages upon change in oxidation state of the TM (due to intercalation or extraction of electroactive species). In terms of fluorine-added polyanionic frameworks that have been explored as Na cathodes, previous studies have focused on fluorophosphates and fluorosulfates [182–185], which predominantly adopt the "tavorite" framework [182, 183]. Na-containing tavorites exhibit a composition of $NaM(XO_4)F$, which is analogous to the Li-containing versions (e.g., $LiFePO_4F$) [185], where M is a TM, and X is P or S. The MO_4F_2 octahedra in tavorites corner-share via F-ions to form a zigzag chain along the *b*-axis, resulting in a triclinic, monoclinic, orthorhombic, or tetragonal symmetry. The oxygens of the MO_4F_2 polyhedra are also shared by XO_4 tetrahedra, which connect pairs of zigzag chains, creating distinct intercalation sites for Na. Note that the structure displayed in Fig. 9(a) is that of orthorhombic-Na_2FePO_4F (*Pbcn* space group), which is available in the inorganic crystal structure database [186].

Both tetragonal ($P4/mmm$) and monoclinic ($C2/c$) $NaVPO_4F$ tavorite frameworks exhibit good electrochemical capacities (132 mAh g^{-1} and 128 mAh g^{-1}, respectively, at 0.1 C), with the monoclinic structure undergoing a reversible transformation to an orthorhombic phase during charging [183]. While the tetragonal polymorph shows a higher voltage (~3.8 V vs. Na compared to 3.4 V in monoclinic) and good cyclability (95.5% capacity retention vs. 78.7% capacity retention in monoclinic over 500 cycles at 1 C), the monoclinic structure displays better rate capability (capacity ~70 mAh g^{-1} at 20 C versus 30 mAh g^{-1} at same rate for tetragonal) [183].

Upon desodiation, orthorhombic-Na_2FePO_4F [Fig. 9(a)] forms $NaFePO_4F$ topotactically, showing a capacity of 100 mAh g^{-1} at 0.1 C when charged between 2.6 and 4 V, involving $Fe^{3+/2+}$ redox [Fig. 9(b)] [187, 188]. Note that 100 mAh g^{-1} represents ~81% of the theoretical capacity of ~124 mAh g^{-1}, corresponding to one mole of Na removal per Na_2FePO_4F formula unit. Theoretical calculations for half desodiation in Na_2FePO_4F, which predict an average intercalation voltage (3.04 V) [189] are in agreement with some experimental studies [190], while higher voltages have also been reported (3.50 V) [191]. Also, the cycling performance of Na_2FePO_4F improved significantly from 60 to 2000 cycles with ~80% capacity retention at 0.1 C, upon particle size reduction and morphological modification [190]. Monoclinic-Na_2MnPO_4F ($P2_1/c$) was investigated using DFT calculations, which predicted facile desodiation up to $NaMnPO_4F$, similar to Na_2FePO_4F, at an average voltage of ~3.76 V vs. Na [192]. However, the calculations predict a high voltage of ~4.8 V for the removal of the second Na (i.e., from $NaMnFePO_4F$ to $MnFePO_4F$), which may be practically difficult due to the lack of suitable electrolytes [192].

Recently, Na-excess fluorophosphates, such as $Na_{1+y}VPO_4F_{1+y}$ ($0 \le y \le 0.5$) [193], $Na_3V_2O_{2x}(PO_4)_2F_{3-2x}$ ($0 \le y \le 1$) [194, 195] and $Na_5M(PO_4)_2F_2$ [196] have been studied as Na cathodes but require further investigation. Among them, $Na_3V_2(PO_4)_2F_3$ (NVPF) [197] from the family of $Na_3V_2O_{2x}(PO_4)_2F_{3-2x}$ compositions, has drawn significant attention due to its high theoretical capacity (128.2 mAh g^{-1} corresponding to two Na extraction) [198]. NVPF crystallizes primarily in an orthorhombic structure with the *Amam* space group [see Fig. 10(a)] [194]. Na occupies Na1 [Wyckoff site: 4c,

pink spheres in Fig. 10(a)] site completely, and Na2 (8f, purple spheres) and Na3 (8f, yellow spheres) sites partially [194].

Experimentally, NVPF displays a reversible capacity of ~ 120 mAh g^{-1} at C/10 (corresponding to exchange of two Na, $Na_3V_2(PO_4)_2F_3 \leftrightarrow NaV_2(PO_4)_2F_3$) at an average voltage of 3.95 V, as shown in Fig. 10(b) [198]. The reversible exchange of Na in $Na_3V_2(PO_4)_2F_3$ is restricted to two moles of Na for two reasons, namely, $NaV_2(PO_4)_2F_3$ is a stable structure with a strong Na-vacancy ordering [199], and desodiation of $NaV_2(PO_4)_2F_3$ irreversibly transitions into tetragonal-$V_2(PO_4)_2F_3$ (space group $I4/mmm$) [200, 201]. The cyclability of NVPF can be improved from 30 cycles at 0.1 C [198] to 1000 cycles at 10 C [202] upon surface modification with graphene. NVPF's capacity is sensitive to the cycling rate, with the structure exhibiting 114 and 80 mAh g^{-1} at 0.5 C and 10 C, respectively [202].

Apart from NVPF, other TM analogs, i.e., $Na_3M_2(PO_4)_2F_3$ for M = Cr, Co and Ni, are predicted to or experimentally display high operating voltages of ~ 5 V for two moles of Na extraction, which may exceed the stability limit of current liquid electrolytes [203]. Other members of $Na_3V_2O_{2x}(PO_4)_2F_{3-2x}$ family (i.e. $0 < x \leq 1$) show reduction in voltage with Na deintercalation as F is increasingly substituted with O [204, 205]. Overall, the chemical space of fluorophosphates has not been yet explored thoroughly as Na cathodes and additional experimental and theoretical studies will help in understanding these systems better and unearth novel and promising candidates.

In terms of fluorosulfates, $NaMSO_4F$ and $Na(M,M')SO_4F$, where M, M′ = Fe, Co, Ni, and Mn, have been synthesized using solid-state (and ionothermal) synthesis protocols to yield monoclinic ($P2_1/c$ or $C2/c$) structures [206, 207]. However, except for $NaFeSO_4F$, which only exhibited ~ 6% of the theoretical capacity (~ 137 mAh g^{-1}) at 3.6 V vs. Na and C/20, the other $NaMSO_4F$ did not show any electrochemical activity [207]. While the initial cause of the lack of electrochemical activity in $NaMSO_4F$ was thought to be the 1D diffusion of Na along the [101] direction in the monoclinic unit cell, the theoretically calculated (using empirical potentials) migration barrier of ~ 0.6 eV in $NaFeSO_4F$ contrastingly indicated fairly robust 1D diffusion [208]. Later experimental work, which utilized a carbon nanotube (CNT)-coated $NaFeSO_4F$ cathode, reported an improved capacity of ~ 110 mAh g^{-1} at 0.1 C with a distinct charging plateau in the 3.6–3.8 V vs. Na window [209]. Further, the CNT coated cathode also displayed reasonable cycling performance (~ 91% capacity retention over 200 cycles at 1 C), and an associated decrease in the charge-transfer resistance measured via impedance spectroscopy, which was largely attributed to an improvement in the electronic conductivity [209]. Thus, strategies to further improve the bulk electronic conductivity, via doping or substitution of the TM in $NaMSO_4F$ [210], may result in improved electrochemical performance from the fluoro-sulfate class of compounds.

Perovskites and rutiles

To fully exploit the inductive effect of F, Na-containing frameworks that have fluorine as the sole anion is pertinent. Typically, a fully sodiated TM fluoride i.e., $NaMF_3$, adopts a

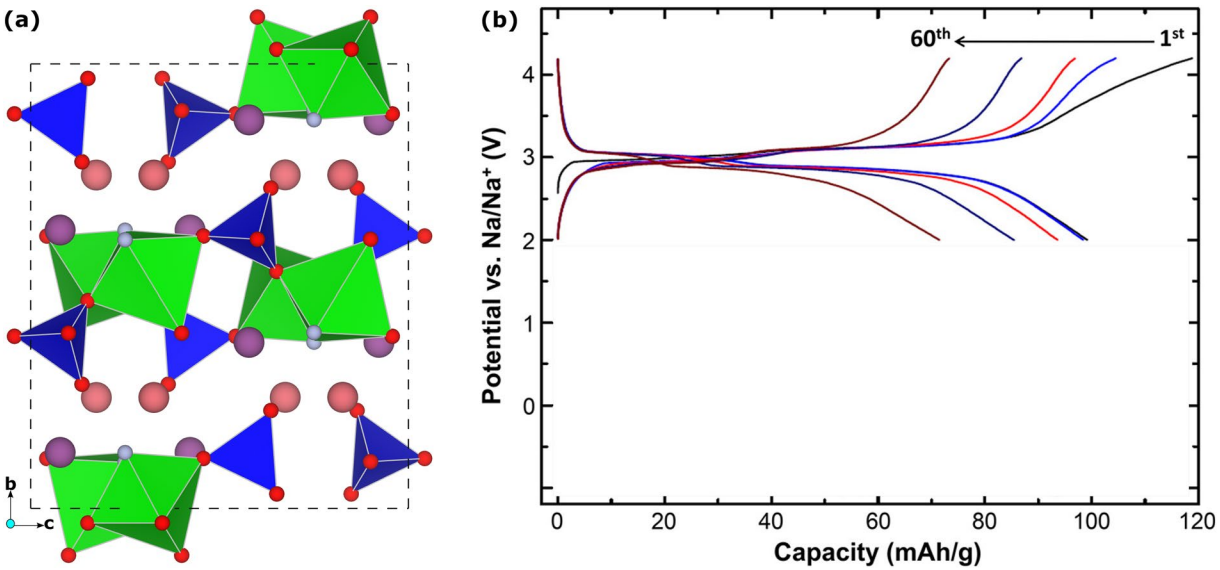

Figure 9: (a) Conventional cell of orthorhombic-Na_2FePO_4F and (b) voltage-capacity profile of topotactic Na exchange from Na_2FePO_4F to form $NaFePO_4F$. Green and blue polyhedra in panel (a) represent TM and P sites, respectively, while pink/purple and red spheres correspond to Na and O atoms. Panel (b) is reproduced from Ref. [187], copyright 2017 American Chemical Society.

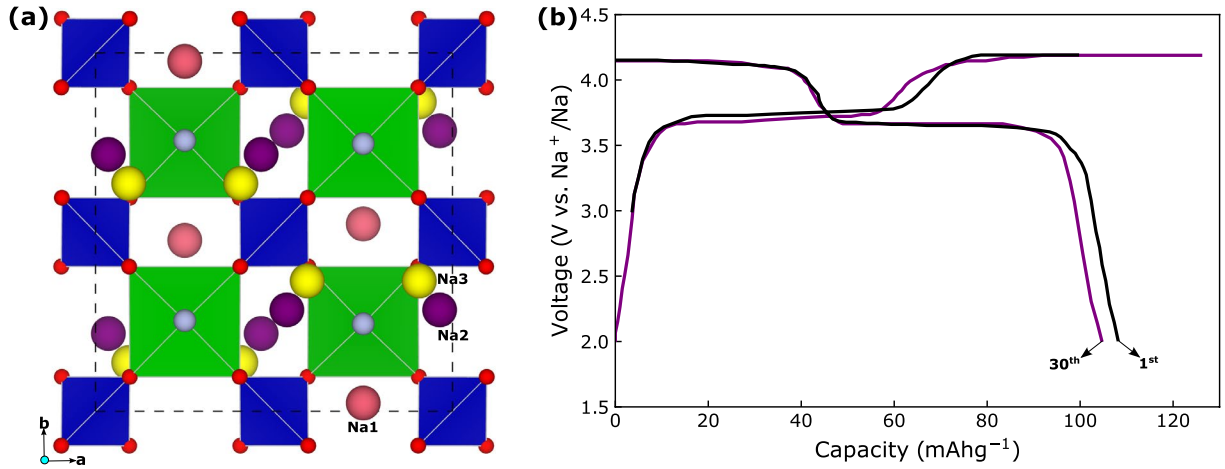

Figure 10: (a) Conventional cell of orthorhombic-$Na_3V_2(PO_4)_2F_3$ and (b) voltage-capacity profile of topotactic Na exchange from $Na_3V_2(PO_4)_2F_3$ to form $NaV_2(PO_4)_2F_3$. Green and blue polyhedra in panel (a) represent TM and P sites, respectively, while pink/purple/yellow, gray and red spheres correspond to Na, F and O atoms. Panel (b) is reproduced from Ref. [198], copyright 2012 Royal Society of Chemistry.

perovskite- or ReO_3-type structure. While the classic cubic perovskite structure consists of corner-sharing MF_6 (or MO_6 in the case of oxide perovskites) octahedra that exhibit large cation "tunnels" at the center of the unit cell [211], Na-containing fluoride perovskite are usually the orthorhombic distorted versions with the *Pmna* space group [Fig. 11(a)]. The ReO_3-type structure is a cubic perovskite with the tunnel-cation sites either unoccupied or partially occupied, with distorted MF_6 (or MO_6) octahedra [Fig. 11(b)]. Other types of fluoride Na-containing frameworks are known, such as weberite-$Na_2Fe_2F_7$ and $NaFeF_4$ [212–218], some of which can be utilized in electrochemical setups [215–218]. Here, we focus on the perovskite-based frameworks.

Although the large cation tunnels in perovskites should theoretically facilitate Na diffusion, so far, only the $NaFeF_3$ perovskite has displayed reasonable electrochemical activity, with a capacity of 200 mAh g^{-1} (which is approximately the theoretical capacity of 197 mAh g^{-1}) at a slow rate of C/10 and an average voltage of 3.10 V vs. Na [215]. Note that contributions from electrolyte decomposition or other side reactions can't be ruled out, yet, in the electrochemical performance reported for $NaFeF_3$. Other TM fluorides, including Mn, Co, and Ni, acted as fluorinating agents or oxidizers, which caused irreversible side reactions with the electrolyte and other components, restricting any potential use in commercial batteries. Moreover, such TM fluorides also exhibit significant structural transformation upon Na extraction [219].

Another pathway to utilize fluorines in cathode frameworks is to explore the chemistry of oxyfluorides, which combines the use of both oxides and fluorides as anions, thereby combining the effects of high voltage (via inductive effect of F^-) and high capacity (due to higher negative charge on O^{2-} resulting in higher amount of intercalate-able Na). Specifically, ordered oxyfluorides that have been explored for Na (de)intercalation either adopt the perovskite framework (e.g., NbO_2F) or the rutile framework [Fig. 11(c)] with $P4_2/mnm$ space group (e.g., $CrO_{2-x}F_x$ and FeO_xF_{2-x}) [220–222]. Electrochemically, rutile-FeOF [223, 224] is claimed to exhibit a Na discharge capacity of 210 mAh g^{-1} for ~ 20 cycles, across a voltage range of 1–4 V vs. Na, corresponding to the $Fe^{4+/3+}$ redox couple. However, FeOF does display significant hysteresis in its voltage-capacity curves, largely due to a (reversible) structural transition from rutile-FeOF to cubic-Na_xFeOF, and the contribution of electrolyte decomposition or other irreversible side reactions to the observed capacity can't be eliminated. Thus, the Na intercalation behavior in rutile-FeOF (and other oxyfluorides) requires deeper investigation [223].

Overall, the chemistry of fluorides and oxyfluorides, which crystallize in perovskite and rutile frameworks, has not been explored in detail, experimentally or theoretically, as Na-ion cathode frameworks. Notably, previous studies have reported the formation of several disordered oxyfluoride frameworks that show promising electrochemical performance in Li-ion cathodes [225, 226]. Such disordered frameworks are theoretically possible within the oxyfluoride chemistry involving Na as well. Specifically, perovskite Na-oxyfluorides, which may exhibit better Na intercalation kinetics than the rutile framework, may form disordered structures that exhibit superior voltages and Na intercalation capacities. Thus, the oxyfluoride space deserves further exploration to identify the next generation of high energy density Na cathodes.

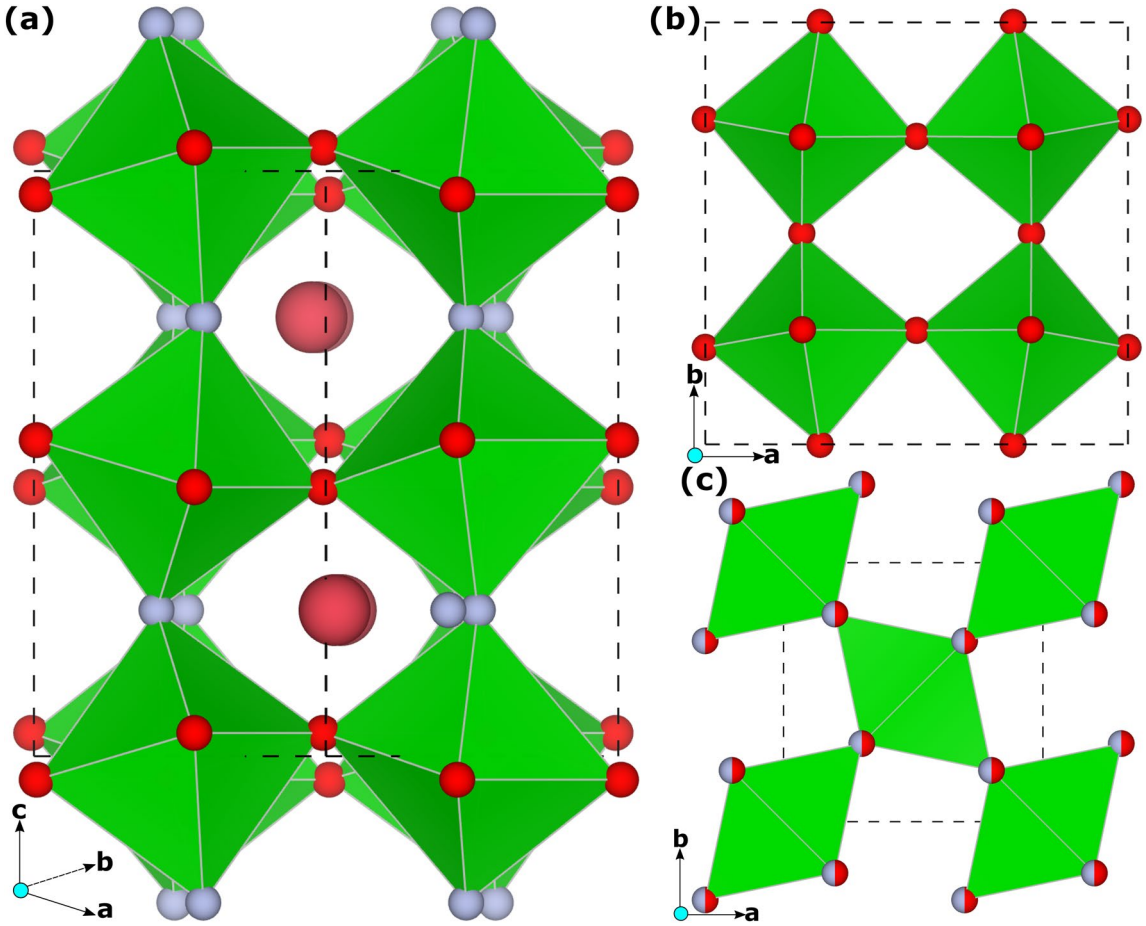

Figure 11: Conventional cells of (a) orthorhombic-perovskite, (b) cubic-ReO_3, and (c) tetragonal-rutile, with green polyhedra representing TM sites and black lines corresponding to unit cell boundaries. Pink, red, and gray spheres in all panels indicate Na, O, and F atoms, respectively. In rutile, the spheres with both red and gray colors indicate disordered configuration of O and F atoms.

Conclusions and outlook

The development of energy storage technologies alternate to the current LIBs, such as the NIB, is an important step to ensure that humanity's energy usage is put on a sustainable course. NIBs hold significant promise, with the earth abundance of Na, the use of Al current collectors, and low self-heating rates, but are challenged by low energy densities, which equal $LiFePO_4$-based commercial LIBs at best. Since the energy density in NIBs are largely dominated by the intercalation electrodes used, especially the cathode, it is crucial to develop robust structural frameworks that can yield both high energy densities and reasonable power performance. Currently, layered TM-based oxides are the SOTA Na cathodes, with robust performance reported using multi-phase (O3 + P2) layered oxides in commercial full and half-cells [15]. However, layered compounds exhibit intrinsic instabilities, particularly at large degrees of Na removal, which cause them to undergo irreversible transitions that eventually affect their electrochemical cycling. Thus, it is crucial to develop intercalation frameworks that remain robust as Na is exchanged from the structure, such as based on polyanionic groups, which is the focus of this work. After providing a brief overview of the layered oxide Na cathodes, we have reviewed here some of the recent progress in the development of novel, polyanionic cathodes for NIBs.

Among polyanionic materials, we have considered various material/structure/mineral types, including NaSICONs, olivines and ortho-polyanions, alluaudites, pyrophosphates, fluoro-polyanions, perovskites, and rutiles. In Table 2, we have summarized performance metrics of a few key polyanionic chemistries, in each material class, which have shown reasonable electrochemical cycling performance. Data from Table 2 is also visually depicted in Fig. 12. Note that several of the polyanion materials compiled in Table 2 involved modifying the particle size of the cathode and/or the surface of the cathode (with carbon-based coating techniques for instance) to improve electronic conductivity. The voltage column in Table 2 includes both the range of voltages (in units of V vs. Na) that experiments scanned and the average voltages during measurements. Both theoretical and

experimentally reported capacities are in units of mAh g^{-1}, with the rates at which the experimental quantities were obtained also included. The penultimate column of Table 2 includes the cycling behavior, given in number of cycles at the cycling rate, with the overall percentage of capacity fade across the number of cycles reported.

The polyanionic classes that exhibit the highest and lowest theoretical capacities are the ortho-polyanions (specifically, orthosilicates), and single-TM NaSICONs, both of which can theoretically exchange 2 Na atoms per f.u., resulting in capacities of ~ 277 and ~ 117 mAh g^{-1}, respectively. However, only ~ 65% of the theoretical capacity in Na_2MnSiO_4 can be utilized experimentally, at low rates of 0.1 C. In fact, the polyanionic frameworks that exhibit high utilization of theoretical capacities are single and mixed-TM NaSICONs (NVP and $Na_xMnCr(PO_4)_3$; ~ 97–98%), pyrophosphates ($Na_{3.12}Mn_{2.44}(P_2O_7)_2$; ~ 97%), fluoro-polyanions ($Na_3V_2(PO_4)_2F_3$; ~ 88.85%), and sulfate alluaudites ($Na_2Fe_2(SO_4)_3$; ~ 90%). On the other hand, olivines (along with ortho-polyanions) exhibit low utilization of theoretical capacities (Na_xFePO_4; ~ 81%). Note that perovskite-$NaFeF_3$ has been claimed to exhibit excess capacity (200 mAh g^{-1}) compared to the theoretical value (~ 197 mAh g^{-1}), which may be due to side reactions that have not been fully understood yet.

Importantly, among the polyanionic classes, single-TM NaSICONs typically show the highest capacity retention at high rates, as signified by NVP, which demonstrates ~ 84% theoretical capacity at high rates (20 C). NVPF has also shown appreciable capacity retention of ~ 75% relative to the first cycle at 10 C. On the other hand, pyrophosphates, and sulfate alluaudites display significant drops in capacity with increasing rates. For example, $Na_{3.12}Mn_{2.44}(P_2O_7)_2$, and $Na_2Fe_2(SO_4)_3$ exhibit only ~ 58%, and 62% of their theoretical capacities, respectively, at elevated rates of 5 C, and 10 C. Additionally, single-TM NaSICONs can also exhibit robust cycling behavior, with NVP displaying a ~ 48% capacity fade over 10,000 cycles (or 0.48% over 100 cycles), while NVPF reported good cyclability of 1000 cycles at 10 C (0.025% loss per cycle). Thus, NaSICONs in general, and single-TM NaSICONs in particular, and the fluorophosphate family of compositions, appear highly promising polyanionic Na intercalation cathodes, with voltages and capacities comparable to layered TM oxides.

The persistent and ongoing challenges for NaSICONs that block them from widespread adoption as Na cathodes are poor electronic conductivity and lower theoretical capacities (compared to layered TM oxides). Researchers are exploring using multiple TM NaSICONs, in addition to applying electron-conducting coatings, as possible strategies to overcome these challenges. Using multiple TMs can also enable the high costs associated with the use of V so that NIBs are cost-competitive with current LIBs. Although mixed TMs, as illustrated by $Na_xMnCr(PO_4)_3$, can show better voltage and experimental capacity than single-TM systems at low rates, their cycling behavior and high-rate performance require significant improvements. Nevertheless, given the robust structural framework [97] and the chemical diversity of the NaSICON space (with doping/elemental mixing possible in both the TM and non-redox-active cation sites), NaSICONs signify a highly promising polyanionic system for developing the next generation of Na intercalation cathodes.

TABLE 2: Summary of electrochemical performance in key electrode compositions across the various polyanionic groups considered.

Cathode class	Space group	Composition	Voltage range (average voltage)	Theoretical capacity	Reported Capacity @ Rate	Cycles @ Rate, Overall capacity Fade	References
NaSICONs	$R\bar{3}m$	$Na_3V_2(PO_4)_3$	2.5–4.0 (3.4)	117 (2 Na^+)	114.2 @0.5C; 98.1 @20C	10,000 @20C, 48%	[75]
		$Na_4MnCr(PO_4)_3$	1.4–4.6 (3.53)	166 (3 Na^+)	160.5 @0.05C; 60.5 @5C	600 @5C, 13.5%	[93]
Olivines	*Pmna*	$NaFePO_4$	2.2–4.3 (2.7)	154 (1 Na^+)	125 @0.05C; 85 @0.5C	50 @0.05C, ~ 8%	[115]
Ortho-polyanions	*Pn*	Na_2MnSiO_4	1.5–4.2 (~ 2.7)	277 (2 Na^+)	182.4 @0.1C; 60.7 @5C	100 @0.1C, 55.3%	[124]
Alluaudites	$P2_1/c$	$Na_2Fe_2(SO_4)_3$	1.9–4.3 (3.8)	120 (2 Na^+)	107.9 @0.1C; 75.1 @10C	300 @0.2C, ~ 10%	[227]
Pyrophosphates	$P\bar{1}$	$Na_{3.12}Mn_{2.44}(P_2O_7)_2$	1.5–4.5 (3.6)	118.1 (2.44 Na^+)	114 @0.1C; 68.1 @5C	500 @5C, 25%	[177]
Fluoro-polyanion	*Amam*	$Na_3V_2(PO_4)_2F_3$	2.0–4.5 (~ 3.95)	128.3 (2 Na^+)	114 @0.5C 80 @10C	1000 @10C, 25%	[202]
Perovskites and Rutiles	*Pnma*	$NaFeF_3$	2.0–4.0 (~ 3.1)	197 (1 Na^+)	200 @0.1C; ~ 100 @25C	100 @25C, ~ 10%	[215]

Voltage range and average voltages are in units of V vs. Na. Theoretical and reported capacities are in mAh g^{-1}, with the cycling rates indicated in terms of C-rates. Cycling behavior is quantified as number of electrochemical cycles at a given cycling rate with the overall capacity fade (in % of initial capacity) across the number of cycles. The final column lists the references from which the data has been compiled.

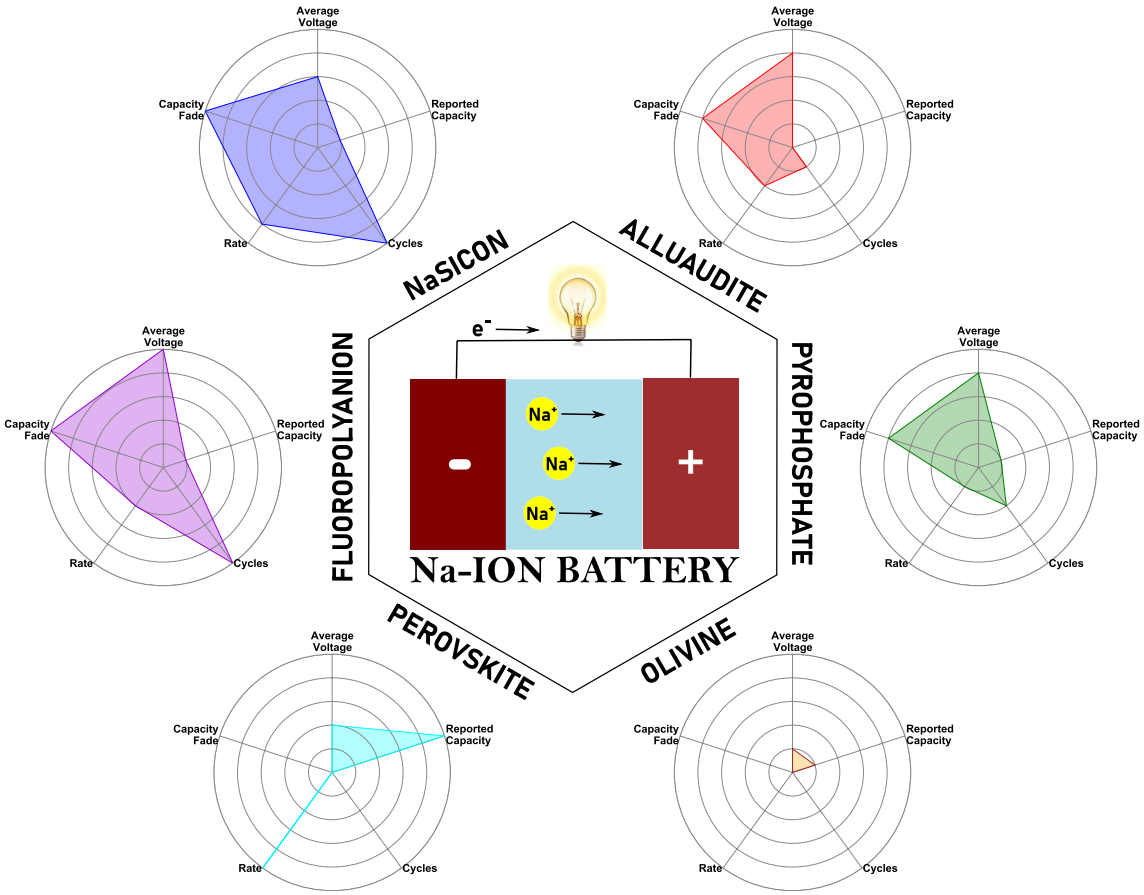

Figure 12: Radar plots summarizing the performance metrics listed in Table 2 for each class of polyanion Na-cathode material. A schematic of a Na battery is presented at the center. Average voltages are normalized such that 0 (origin) represents ≤ 2.5 V vs. Na and 1 (largest circle) signifies ≥ 4.0 V. Similarly, experimentally reported capacity, maximum number of cycles, highest rate performance demonstrated experimentally, and capacity fade per cycle are normalized over the ranges of 100–200 mAh g^{-1}, 100–1000 cycles, 1–25 C, and 0.1%-0.03%, respectively. Intermediate circles are linearly interpolated between the extreme values. For NaSICON, we used the values corresponding to NVP.

Poor electronic conductivity of the bulk cathode is a major bottleneck for almost all Na-based polyanionic systems to overcome, since it can cause poor rate and/or cycle performance. Across most of the experimental literature concerning polyanionic Na cathodes, we observed that a common strategy to improve the electronic conductivity is not to change the bulk electrode composition but rather vary the particle size (micron-sized to nanosized), the particle morphology (different particle arrangements and architectures), and/or the particle surface (via carbon-based or similar coatings). While these are reasonable strategies that can be used to improve electrochemical performance at the lab-scale, implementing such size/morphology/surface optimizations at the commercial scale may have additional levels of challenges. Moreover, such particle-level optimizations typically result in capacity gains at low voltages vs. Na. One practical alternative is to change or optimize the bulk composition of the electrode, by adding other elements and/or controlling the range of Na contents across with (de)intercalation occurs, which can alter the bulk electronic properties of the cathode. For example, activating the $V^{3+/2+}$ redox couple (i.e., Na exchange between $Na_3V_2(PO_4)_3$ and $Na_4V_2(PO_4)_3$) has been theoretically shown to cause a significant drop in the band gap of NVP [228]. Similarly, theoretical calculations have also predicted significant changes in the band gap of $NaMSO_4F$ compounds via mixing of multiple TMs [210]. Hence, we urge the experimental (and theoretical) community to not abandon such approaches to improve electrochemical performance of polyanion cathodes.

Apart from practical usage of polyanionic Na intercalation hosts, significant amount of work is still remaining to fully understand the fundamental phase behavior and Na intercalation mechanisms in these frameworks, which nominally require in-depth characterization techniques (e.g., in operando diffraction and spectroscopy) and theoretical calculations (e.g., building lattice models). For instance, a recent experimental study has demonstrated the existence of $Na_2V_2(PO_4)_3$ [229] a unique Na-vacancy ordering in the NVP system, which was predicted theoretically earlier [228].

The Na intercalation behavior in Na_xFePO_4 is experimentally observed (and also theoretically predicted) to be significantly different from the Li-intercalation behavior in Li_xFePO_4, which requires further investigation. Additionally, the Na intercalation (or the occurrence of other side reactions) is yet to be fully understood in fluorine-based chemical spaces, such as fluoro-polyanions, perovskites, and rutiles. Devoting the effort to better understand the fundamental thermodynamics and kinetics of different systems can provide clarity while searching for novel candidates and also shorten the time scale of optimization in taking a given material from lab to commercial scale. We hope that with efforts directed at both screening of new candidates and improving the understanding of how existing materials work, the scientific community will progress swiftly towards the development of the next generation of NIBs that are powered by polyanionic cathodes.

Acknowledgments

G.S.G. acknowledges financial support from the Indian Institute of Science (IISc) Seed Grant, SG/MHRD/20/0020 and SR/MHRD/20/0013 and the Science and Engineering Research Board (SERB) of the Department of Science and Technology, Government of India, under sanction numbers SRG/2021/000201 and IPA/2021/000007. D.D. thanks the Ministry of Human Resource Development, Government of India, for financial assistance.

Data availability

All data analyzed in this study are already included within the article text, figures, and tables, and are part of prior published literature.

Declarations

Conflict of interest The authors declare no conflicts of interest associated with this work.

References

1. T. Chen, Y. Jin, H. Lv, A. Yang, M. Liu, B. Chen, Y. Xie, Q. Chen, Applications of lithium-ion batteries in grid scale energy storage systems. Trans. Tianjin Univ. **26**, 208 (2020)
2. Y. Ding, Z.P. Cano, A. Yu, J. Lu, Z. Chen, Automotive Li-ion batteries: Current status and future perspectives. Electrochem. Energy Rev. **2**(1), 1 (2019)
3. G. Zubi, R. Dufo-López, M. Carvalho, G. Pasaoglu, The lithium-ion battery: State of the art and future perspectives. Renew. Sustain. Energy Rev. **89**, 292 (2018)
4. H. Epstein, S.M. O'Flarity, Considerations for reducing aviation's CO_2 with aircraft electric propulsion. J. Propul. Power **35**(3), 572 (2019)
5. S. Sripad, V. Viswanathan, Evaluation of current, future, and beyond Li-ion batteries for the electrification of light commercial vehicles: Challenges and opportunities. J. Electrochem. Soc. **164**(11), E3635 (2017)
6. J.B. Quinn, T. Waldmann, K. Richter, M. Kasper, M. Wohlfahrt-Mehrens, Energy density of cylindrical Li-ion cells: A comparison of commercial 18650 to the 21700 cells. J. Electrochem. Soc. **165**(14), A3284 (2018)
7. M.S. Whittingham, History, evolution, and future status of energy storage. Proc. IEEE **100**, 1518 (2012)
8. M.S. Whittingham, Ultimate limits to intercalation reactions for lithium batteries. Chem. Rev. **114**(23), 11414 (2014)
9. G. Assat, J.M. Tarascon, Fundamental understanding and practical challenges of anionic redox activity in Li-ion batteries. Nat. Energy **3**(5), 373 (2018)
10. M. Naor, N. Adler, G.D. Pinto, A. Dumanis, Psychological safety in aviation new product development teams: Case study of 737 max airplane. Sustainability **12**(21), 8994 (2020)
11. Q. Zhao, Y. Lu, J. Chen, Advanced organic electrode materials for rechargeable sodium-ion batteries. Adv. Energy Mater. **7**(8), 1601792 (2017)
12. C. Vaalma, D. Buchholz, M. Weil, S. Passerini, A cost and resource analysis of sodium-ion batteries. Nat. Rev. Mater. **3**(4), 18013 (2018)
13. K. Chayambuka, G. Mulder, D.L. Danilov, P.H.L. Notten, From Li-Ion batteries toward Na-ion chemistries: Challenges and opportunities. Adv. Energy Mater. **10**(38), 2001310 (2020)
14. C. Delmas, Sodium and sodium-ion batteries: 50 years of research. Adv. Energy Mater. **8**(17), 1703137 (2018)
15. A. Rudola, A.J.R. Rennie, R. Heap, S.S. Meysami, A. Lowbridge, F. Mazzali, R. Sayers, C.J. Wright, J. Barker, Commercialisation of high energy density sodium-ion batteries: Faradion's journey and outlook. J. Mater. Chem. A **9**(13), 8279 (2021)
16. T. Liu, X. Yang, J. Nai, Y. Wang, Y. Liu, C. Liu, X. Tao, Recent development of Na metal anodes: Interphase engineering chemistries determine the electrochemical performance. Chem. Eng. J. **409**, 127943 (2021)
17. C. Delmas, D. Carlier, M. Guignard, The layered oxides in lithium and sodium-ion batteries: A solid-state chemistry approach. Adv. Energy Mater. **11**(2), 2001201 (2021)
18. B. Wang, Y. Han, X. Wang, N. Bahlawane, H. Pan, M. Yan, Y. Jiang, Prussian blue analogs for rechargeable batteries. ISci. **3**, 110 (2018)
19. X. Wu, C. Wu, C. Wei, L. Hu, J. Qian, Y. Cao, X. Ai, J. Wang, H. Yang, Highly crystallized $Na_2CoFe(CN)_6$ with suppressed lattice defects as superior cathode material for sodium-ion batteries. ACS Appl. Mater. Interfaces **8**(8), 5393 (2016)

20. T. Jin, H. Li, K. Zhu, P.F. Wang, P. Liu, L. Jiao, Polyanion-type cathode materials for sodium-ion batteries. Chem. Soc. Rev. **49**, 2342 (2020)
21. S.-W. Kim, D.-H. Seo, X. Ma, G. Ceder, K. Kang, Electrode materials for rechargeable sodium-ion batteries: Potential alternatives to current lithium-ion batteries. Adv. Energy Mater. **2**(7), 710 (2012)
22. P.F. Wang, Y. You, Y.X. Yin, Y.G. Guo, Layered oxide cathodes for sodium-ion batteries: Phase transition, air stability, and performance. Adv. Energy Mater. **8**(8), 1701912 (2018)
23. B. Senthilkumar, C. Murugesan, L. Sharma, S. Lochab, P. Barpanda, An overview of mixed polyanionic cathode materials for sodium-ion batteries. Small Methods **3**(4), 1800253 (2019)
24. S.K. Sapra, J. Pati, P.K. Dwivedi, S. Basu, J.K. Chang, R.S. Dhaka, A comprehensive review on recent advances of polyanionic cathode materials in Na-ion batteries for cost effective energy storage applications. Wiley Interdiscip. Rev.: Energy Environ. **10**(5), 400 (2021)
25. P. Barpanda, L. Lander, S.I. Nishimura, A. Yamada, Polyanionic insertion materials for sodium-ion batteries. Adv. Energy Mater. **8**(17), 1703055 (2018)
26. Q. Zhang, Z. Yu, P. Du, C. Su, Carbon nanomaterials used as conductive additives in lithium ion batteries. Recent Pat. Nanotechnol. **4**(2), 100 (2010)
27. T.L. Shao, C. Liu, W. Deng, C. Li, X. Wang, M. Xue, R. Li, Metal oxide-based supercapacitors: Progress and prospectives. Batteries Supercaps **1**(12), 4644 (2019)
28. P. Hohenberg, W. Kohn, Inhomogeneous electron gas. Phys. Rev. **136**(3B), B864 (1964)
29. W. Kohn, L.J. Sham, Self-consistent equations including exchange and correlation effects. Phys. Rev. **140**(4A), 1133 (1965)
30. X. He, Y. Zhu, A. Epstein, Y. Mo, Statistical variances of diffusional properties from ab initio molecular dynamics simulations. NPJ Comput. Mater. **4**, 18 (2018)
31. G. Henkelman, G. Jóhannesson, H. Jónsson, *Progress on Theoretical Chemistry and Physics* (Kluwer Academic, Switzerland, 2006), pp. 269–302
32. S. Adams, R.P. Rao, Understanding ionic conduction and energy storage materials with bond-valence-based methods. Struct. Bond. **158**, 129 (2014)
33. P. Canepa, G. Sai Gautam, D.C. Hannah, R. Malik, M. Liu, K.G. Gallagher, K.A. Persson, G. Ceder, Odyssey of multivalent cathode materials: Open questions and future challenges. Chem. Rev. **117**(5), 4287 (2017)
34. Y. Gao, T.P. Mishra, S.-H. Bo, G. Sai Gautam, P. Canepa, Design and characterization of host-frameworks for facile magnesium transport. Ann. Rev. Mater. Res. **52**, 129 (2022)
35. J.L. Kaufman, J. Vinckevičiūtė, S. Krishna Kolli, J. Gabriel Goiri, A. van der Ven, Understanding intercalation compounds for sodium-ion batteries and beyond. Philos. Trans. R. Soc. Lond. Ser. A **377**(2152), 20190020 (2019)
36. C. Delmas, C. Fouassier, P. Hagenmuller, Structural classification and properties of the layered oxides. Physica B+C **99**(1–4), 81 (1980)
37. J. Manzi, A. Paolone, O. Palumbo, D. Corona, A. Massaro, R. Cavaliere, A.B. Muñoz-García, F. Trequattrini, M. Pavone, S. Brutti, Monoclinic and orthorhombic $NaMnO_2$ for secondary batteries: A comparative study. Energies **14**(5), 1230 (2021)
38. M.H. Han, E. Gonzalo, M. Casas-Cabanas, T. Rojo, Structural evolution and electrochemistry of monoclinic $NaNiO_2$ upon the first cycling process. J. Power Sources **258**, 266 (2014)
39. X. Li, Y. Wang, D. Wu, L. Liu, S.-H. Bo, G. Ceder, Jahn-Teller assisted Na diffusion for high performance Na ion batteries. Chem. Mater. **28**(18), 6575 (2016)
40. L. Vitoux, M. Guignard, N. Penin, D. Carlier, J. Darriet, C. Delmas, $NaMoO_2$: A layered oxide with molybdenum clusters. Inorg. Chem. **59**(6), 4015 (2020)
41. J. Vinckevičiūtė, M. D. Radin, A. Ben, Stacking-sequence changes and Na ordering in layered intercalation materials. Chem. Mater. **28**(23), 8640 (2016)
42. T. Ma, G.-L. Xu, X. Zeng, Y. Li, Y. Ren, C. Sun, S.M. Heald, J. Jorne, K. Amine, Z. Chen, Solid state synthesis of layered sodium manganese oxide for sodium-ion battery by in-situ high energy X-ray diffraction and X-ray absorption near edge spectroscopy. J. Power Sources **341**, 114 (2017)
43. K. Kubota, I. Ikeuchi, T. Nakayama, C. Takei, N. Yabuuchi, H. Shiiba, M. Nakayama, S. Komaba, New insight into structural evolution in layered $NaCrO_2$ during electrochemical sodium extraction. J. Phys. Chem. C **119**(1), 166 (2015)
44. Y. Lei, X. Li, L. Liu, G. Ceder, Synthesis and stoichiometry of different layered sodium cobalt oxides. Chem. Mater. **26**(18), 5288 (2014)
45. A.J. Toumar, S.P. Ong, W.D. Richards, S. Dacek, G. Ceder, Vacancy ordering in O3-type layered metal oxide sodium-ion battery cathodes. Phys. Rev. Appl. **4**(6), 64002 (2015)
46. J.L. Kaufman, A. van der Ven, Na_xCoO_2 phase stability and hierarchical orderings in the O3/P3 structure family. Phys. Rev. Mater. **3**(1), 15402 (2019)
47. M.D. Radin, J. Alvarado, Y.S. Meng, A. van der Ven, Role of crystal symmetry in the reversibility of stacking-sequence changes in layered intercalation electrodes. Nano Lett. **17**(12), 7789 (2017)
48. D. Hamani, M. Ati, J.M. Tarascon, P. Rozier, Na_xVO_2 as possible electrode for Na-ion batteries. Electrochem. Commun. **13**(9), 938 (2011)
49. A. Caballero, L. Hernán, J. Morales, L. Sánchez, J. Santos Peña, M.A.G. Aranda, Synthesis and characterization of high-temperature hexagonal P2-$Na_{0.6}MnO_2$ and its electrochemical behaviour as cathode in sodium cells. J. Mater. Chem. **12**(4), 1142 (2002)

50. B.V.R. Reddy, R. Ravikumar, C. Nithya, S. Gopukumar, High performance Na_xCoO_2 as a cathode material for rechargeable sodium batteries. J. Mater. Chem. A **3**(35), 18059 (2015)
51. C.A. Marianetti, G. Kotliar, Na-induced correlations in Na_xCoO_2. Phys. Rev. Lett. **98**(17), 176405 (2007)
52. C. Delmas, J.-J. Braconnier, C. Fouassier, P. Hagenmuller, Electrochemical intercalation of sodium in Na_xCoO_2 bronzes. Solid State Ionics **3–4**, 165 (1981)
53. M. Bianchini, J. Wang, R. Clément, G. Ceder, A first-principles and experimental investigation of nickel solubility into the P2 Na_xCoO_2 sodium-ion cathode. Adv. Energy Mater. **8**(26), 1801446 (2018)
54. F. Tournadre, L. Croguennec, I. Saadoune, D. Carlier, Y. Shao-Horn, P. Willmann, C. Delmas, On the mechanism of the P2-$Na_{0.70}CoO_2$→O2-$LiCoO_2$ exchange reaction - Part I: Proposition of a model to describe the P2–O2 transition. J. Solid State Chem. **177**(8), 2790 (2004)
55. H. Liu, X. Gao, J. Chen, J. Gao, S. Yin, S. Zhang, L. Yang, S. Fang, Y. Mei, X. Xiao, L. Chen, W. Deng, F. Li, G. Zou, H. Hou, X. Ji, Reversible OP4 phase in P2–$Na_{2/3}Ni_{1/3}Mn_{2/3}O_2$ sodium ion cathode. J. Power Sources **508**, 230324 (2021)
56. A. Kulka, C. Marino, K. Walczak, C. Borca, C. Bolli, P. Novák, C. Villevieille, Influence of Na/Mn arrangements and P2/P′2 phase ratio on the electrochemical performance of Na_xMnO_2 cathodes for sodium-ion batteries. J. Mater. Chem. A **8**(12), 6022 (2020)
57. Y. Mo, S.P. Ong, G. Ceder, Insights into diffusion mechanisms in P2 layered oxide materials by first-principles calculations. Chem. Mater. **26**(18), 5208 (2014)
58. Y. Hinuma, Y.S. Meng, G. Ceder, Temperature-concentration phase diagram of P2-Na_xCoO_2 from first-principles calculations. Phys. Rev. B **77**(22), 224111 (2008)
59. D.H. Lee, J. Xu, Y.S. Meng, An advanced cathode for Na-ion batteries with high rate and excellent structural stability. Phys. Chem. Chem. Phys. **15**(9), 3304 (2013)
60. R. Sayers, J. Barker, R. Heap, Compositions containing doped nickelate compounds. *US10196280B2* (Faradion Ltd, 2019)
61. D. Wu, X. Li, B. Xu, N. Twu, L. Liu, G. Ceder, $NaTiO_2$: A layered anode material for sodium-ion batteries. Energy Environ. Sci. **8**(1), 195 (2015)
62. N. Yabuuchi, H. Yoshida, S. Komaba, Crystal structures and electrode performance of alpha-$NaFeO_2$ for rechargeable sodium batteries. Electrochemistry **80**(10), 716 (2012)
63. B. Singh, Z. Wang, S. Park, G.S. Gautam, J.N. Chotard, L. Croguennec, D. Carlier, A.K. Cheetham, C. Masquelier, P. Canepa, A chemical map of NaSICON electrode materials for sodium-ion batteries. J. Mater. Chem. A **9**(1), 281 (2021)
64. J.N. Chotard, G. Rousse, R. David, O. Mentré, M. Courty, C. Masquelier, Discovery of a sodium-ordered form of $Na_3V_2(PO_4)_3$ below ambient temperature. Chem. Mater. **27**(17), 5982 (2015)
65. Z. Deng, T. P. Mishra, E. Mahayoni, Q. Ma, O. Guillon, J-N. Chotard, V. Seznec, A. K. Cheetham, C. Masquelier, G. S. Gautam, P. Canepa, Theoretical and Experimental Studies of Ion Transport in Mixed Polyanion Solid Electrolytes. *Under Review*, (n.d.).
66. Z. Zou, N. Ma, A. Wang, Y. Ran, T. Song, Y. Jiao, J. Liu, H. Zhou, W. Shi, B. He, D. Wang, Y. Li, M. Avdeev, S. Shi, Relationships between Na^+ distribution, concerted migration, and diffusion properties in rhombohedral NASICON. Adv. Energy Mater. **10**(30), 2001486 (2020)
67. Y. Ishado, A. Inoishi, S. Okada, Exploring factors limiting three-Na^+ extraction from $Na_3V_2(PO_4)_3$. Electrochemistry **88**(5), 457 (2020)
68. Z. Zhang, Z. Zou, K. Kaup, R. Xiao, S. Shi, M. Avdeev, Y.S. Hu, D. Wang, B. He, H. Li, X. Huang, L.F. Nazar, L. Chen, Correlated migration invokes higher Na^+-ion conductivity in NaSICON-type solid electrolytes. Adv. Energy Mater. **9**(42), 1902373 (2019)
69. S.Y. Lim, H. Kim, R.A. Shakoor, Y. Jung, J.W. Choi, Electrochemical and thermal properties of NASICON structured $Na_3V_2(PO_4)_3$ as a sodium rechargeable battery cathode: A combined experimental and theoretical study. J. Electrochem. Soc. **159**(9), A1393 (2012)
70. Z. Jian, L. Zhao, H. Pan, Y.S. Hu, H. Li, W. Chen, L. Chen, Carbon coated $Na_3V_2(PO_4)_3$ as novel electrode material for sodium ion batteries. Electrochem. Commun. **14**(1), 86 (2012)
71. X. Yao, Z. Zhu, Q. Li, X. Wang, X. Xu, J. Meng, W. Ren, X. Zhang, Y. Huang, L. Mai, High energy density symmetric sodium-ion battery: $Na_4V_2(PO_4)_3$‖$Na_3V_2(PO_4)_3$. ACS Appl. Mater. Interfaces **10**(12), 10022 (2018)
72. L. Bi, X. Li, X. Liu, Q. Zheng, D. Lin, Enhanced cycling stability and rate capability in a La-doped $Na_3V_2(PO_4)_3$/C cathode for high-performance sodium ion batteries. ACS Sustain. Chem. Eng. **7**(8), 7693 (2019)
73. S. Sun, Y. Chen, J. Cheng, Z. Tian, C. Wang, G. Wu, C. Liu, Y. Wang, L. Guo, Constructing dimensional gradient structure of $Na_3V_2(PO_4)_3$/C@CNTs-WC by wolfram substitution for superior sodium storage. Chem. Eng. J. **420**(3), 130453 (2021)
74. X. Li, Y. Huang, J. Wang, L. Miao, Y. Li, Y. Liu, Y. Qiu, C. Fang, J. Han, Y. Huang, High valence Mo-doped $Na_3V_2(PO_4)_3$/C as a high rate and stable cycle-life cathode for sodium battery. J. Mater. Chem. A **6**(4), 1390 (2018)
75. Y. Zhao, X. Cao, G. Fang, Y. Wang, H. Yang, S. Liang, A. Pan, G. Cao, Hierarchically carbon-coated $Na_3V_2(PO_4)_3$ nanoflakes for high-rate capability and ultralong cycle-life sodium ion batteries. Chem. Eng. J. **339**, 162 (2018)
76. Q. Zhu, X. Chang, N. Sun, H. Liu, R. Chen, F. Wu, B. Xu, Microorganism-moulded pomegranate-like $Na_3V_2(PO_4)_3$/C nanocomposite for advanced sodium-ion batteries. J. Mater. Chem. A **5**(20), 9982 (2017)

77. L. Zhao, H. Zhao, X. Long, Z. Li, Z. Du, Superior high-rate and ultralong-lifespan $Na_3V_2(PO_4)_3$ @C cathode by enhancing the conductivity both in bulk and on surface. ACS Appl. Mater. Interfaces **10**(42), 35963 (2018)
78. X. Liu, G. Feng, E. Wang, H. Chen, Z. Wu, W. Xiang, Y. Zhong, Y. Chen, X. Guo, B. Zhong, Insight into preparation of Fe-doped $Na_3V_2(PO_4)_3$ @C from aspects of particle morphology design, crystal structure modulation, and carbon graphitization regulation. ACS Appl. Mater. Interfaces **11**(13), 12421 (2019)
79. K. Kawai, W. Zhao, S.I. Nishimura, A. Yamada, High-voltage Cr^{4+}/Cr^{3+} redox couple in polyanion compounds. ACS Appl. Energy Mater. **1**(3), 928 (2018)
80. S. Park, J.N. Chotard, D. Carlier, I. Moog, M. Courty, M. Duttine, F. Fauth, A. Iadecola, L. Croguennec, C. Masquelier, Crystal structures and local environments of NASICON-type $Na_3V_2(PO_4)_3$ and $Na_4V_2(PO_4)_3$ positive electrode materials for Na-Ion batteries. Chem. Mater. **33**(13), 5355 (2021)
81. Y. Zhao, X. Gao, H. Gao, H. Jin, J.B. Goodenough, Three electron reversible redox reaction in sodium vanadium chromium phosphate as a high-energy-density cathode for sodium-ion batteries. Adv. Funct. Mater. **30**(10), 1908680 (2020)
82. C. Delmas, F. Cherkaoui, A. Nadiri, P. Hagenmuller, A nasicon-type phase as intercalation electrode: $NaTi_2(PO_4)_3$. Mater. Res. Bull. **22**(5), 631 (1987)
83. P. Senguttuvan, G. Rousse, M.E. Arroyo, Y. De Dompablo, H. Vezin, J.M. Tarascon, M.R. Palacín, Low-potential sodium insertion in a NASICON-type structure through the Ti(III)/Ti(II) redox couple. J. Am. Chem. Soc. **135**(10), 3897 (2013)
84. R. Rajagopalan, B. Chen, Z. Zhang, X.L. Wu, Y. Du, Y. Huang, B. Li, Y. Zong, J. Wang, G.H. Nam, M. Sindoro, S.X. Dou, H.K. Liu, H. Zhang, Improved reversibility of Fe^{3+}/Fe^{4+} redox couple in sodium super ion conductor type $Na_3Fe_2(PO_4)_3$ for sodium-ion batteries. Adv. Mater. **29**(12), 1605694 (2017)
85. J. Gopalakrishnan, K.K. Rangan, Vanadium phosphate ($V_2(PO_4)_3$): A novel NASICON-type vanadium phosphate synthesized by oxidative deintercalation of sodium from sodium vanadium phosphate ($Na_3V_2(PO_4)_3$). Chem. Mater. **4**(4), 745 (1992)
86. S. Il Park, I. Gocheva, S. Okada, J. Yamaki, Electrochemical properties of $NaTi_2(PO_4)_3$ anode for rechargeable aqueous sodium-ion batteries. J. Electrochem. Soc. **158**(10), A1067 (2011)
87. S.C. Chung, J. Ming, L. Lander, J. Lu, A. Yamada, Rhombohedral NASICON-type $Na_xFe_2(SO_4)_3$ for sodium ion batteries: Comparison with phosphate and alluaudite phases. J. Mater. Chem. A **6**(9), 3919 (2018)
88. X. Ma, X. Cao, Y. Zhou, S. Guo, X. Shi, G. Fang, A. Pan, B. Lu, J. Zhou, S. Liang, Tuning crystal structure and redox potential of NASICON-type cathodes for sodium-ion batteries. Nano Res. **13**(12), 3330 (2020)
89. W. Zhou, L. Xue, X. Lü, H. Gao, Y. Li, S. Xin, G. Fu, Z. Cui, Y. Zhu, J.B. Goodenough, $Na_xMV(PO_4)_3$ (M = Mn, Fe, Ni) structure and properties for sodium extraction. Nano Lett. **16**(12), 7836 (2016)
90. R. Chen, D.S. Butenko, S. Li, D. Li, X. Zhang, J. Cao, I.V. Ogorodnyk, N.I. Klyui, W. Han, I.V. Zatovsky, Effects of low doping on the improvement of cathode materials $Na_{3+x}V_{2-x}M_x(PO_4)_3$ (M = Co^{2+}, Cu^{2+}; x = 0.01–0.05) for SIBs. J. Mater. Chem. A **9**(32), 17380 (2021)
91. S. Ghosh, N. Barman, E. Gonzalez-Correa, M. Mazumder, A. Zaveri, R. Giovine, A. Manche, S.K. Pati, R.J. Clément, P. Senguttuvan, Elucidating the impact of Mg substitution on the properties of NASICON-$Na_{3+y}V_{2-y}Mg_y(PO_4)_3$ cathodes. Adv. Funct. Mater. **31**(48), 2105463 (2021)
92. F. Lalère, V. Seznec, M. Courty, J.N. Chotard, C. Masquelier, Coupled X-ray diffraction and electrochemical studies of the mixed Ti/V-containing NASICON: $Na_2TiV(PO_4)_3$. J. Mater. Chem. A **6**(15), 6654 (2018)
93. J. Zhang, Y. Liu, X. Zhao, L. He, H. Liu, Y. Song, S. Sun, Q. Li, X. Xing, J. Chen, A novel NASICON-type $Na_4MnCr(PO_4)_3$ demonstrating the energy density record of phosphate cathodes for sodium-ion batteries. Adv. Mater. **32**(11), 1906348 (2020)
94. T. Zhu, P. Hu, X. Wang, Z. Liu, W. Luo, K.A. Owusu, W. Cao, C. Shi, J. Li, L. Zhou, L. Mai, Realizing three-electron redox reactions in NASICON-structured $Na_4MnTi(PO_4)_3$ for sodium-ion batteries. Adv. Energy Mater. **9**(9), 1803436 (2019)
95. J. Zhang, C. Lin, Q. Xia, C. Wang, X.S. Zhao, Improved performance of $Na_3TiMn(PO_4)_3$ using a non-stoichiometric synthesis strategy. ACS Energy Lett. **6**(6), 2081 (2021)
96. Z. Zhang, S. Wenzel, Y. Zhu, J. Sann, L. Shen, J. Yang, X. Yao, Y.-S. Hu, C. Wolverton, H. Li, L. Chen, J. Janek, $Na_3Zr_2Si_2PO_{12}$: A stable Na^+-ion solid electrolyte for solid-state batteries. ACS Appl. Energy Mater. **3**(8), 7427 (2020)
97. Z. Deng, G. Sai Gautam, S.K. Kolli, J.N. Chotard, A.K. Cheetham, C. Masquelier, P. Canepa, Phase behavior in rhombohedral NaSiCON electrolytes and electrodes. Chem. Mater. **32**(18), 7908 (2020)
98. L.X. Yuan, Z.H. Wang, W.X. Zhang, X.L. Hu, J.T. Chen, Y.H. Huang, J.B. Goodenough, Development and challenges of $LiFePO_4$ cathode material for lithium-ion batteries. Energy Environ. Sci. **4**(2), 269 (2011)
99. C. Heubner, S. Heiden, M. Schneider, A. Michaelis, In-situ preparation and electrochemical characterization of submicron sized $NaFePO_4$ cathode material for sodium-ion batteries. Electrochim. Acta **233**, 78 (2017)
100. T. Boyadzhieva, V. Koleva, E. Zhecheva, D. Nihtianova, L. Mihaylov, R. Stoyanova, Competitive lithium and sodium intercalation into sodium manganese phospho-olivine $NaMnPO_4$ covered with carbon black. RSC Adv. **5**(106), 87694 (2015)

101. M. MinakshiSundaram, D.R.G. Mitchell, Dispersion of Ni^{2+} ions: Via acetate precursor in the preparation of $NaNiPO_4$ nanoparticles: Effect of acetate vs. nitrate on the capacitive energy storage properties. Dalton Trans. **46**(40), 13704 (2017)
102. K. Kaliyappan, Z. Chen, Facile solid-state synthesis of eco-friendly sodium iron silicate with exceptional sodium storage behaviour. Electrochim. Acta **283**, 1384 (2018)
103. L. Zhu, L. Li, J. Wen, Y.R. Zeng, Structural stability and ionic transport property of $NaMPO_4$ (M = V, Cr, Mn, Fe Co, Ni) as cathode material for Na-ion batteries. J. Power Sources **438**, 227016 (2019)
104. S.P. Ong, V.L. Chevrier, G. Hautier, A. Jain, C. Moore, S. Kim, X. Ma, G. Ceder, Voltage, stability and diffusion barrier differences between sodium-ion and lithium-ion intercalation materials. Energy Environ. Sci. **4**(9), 3680 (2011)
105. G. Ali, J.-H. Lee, D. Susanto, S.-W. Choi, B.W. Cho, K.-W. Nam, K.Y. Chung, Polythiophene-wrapped olivine $NaFePO_4$ as a cathode for Na-ion batteries. ACS Appl. Mater. Interfaces **8**(24), 15422 (2016)
106. A.J. Fernández-Ropero, D. Saurel, B. Acebedo, T. Rojo, M. Casas-Cabanas, Electrochemical characterization of $NaFePO_4$ as positive electrode in aqueous sodium-ion batteries. J. Power Sources **291**, 40 (2015)
107. T. Boyadzhieva, V. Koleva, R. Stoyanova, Crystal chemistry of Mg substitution in $NaMnPO_4$ olivine: Concentration limit and cation distribution. Phys. Chem. Chem. Phys. **19**(20), 12730 (2017)
108. T. Boyadzhieva, V. Koleva, R. Kukeva, D. Nihtianova, S. Harizanova, R. Stoyanova, Storage performance of Mg^{2+} substituted $NaMnPO_4$ with an olivine structure. RSC Adv. **10**(49), 29051 (2020)
109. R. Malik, A. Abdellahi, G. Ceder, A critical review of the Li insertion mechanisms in $LiFePO_4$ electrodes. J. Electrochem. Soc. **160**(5), A3179 (2013)
110. L. Zhao, D. Zhou, W. Huang, X. Kang, Q. Shi, Z. Deng, X. Yan, Y. Yu, Electrochemical performances of maricite $NaFePO_4$/C as cathode material for sodium-ion and lithium-ion batteries. Int. J. Electrochem. Sci. **12**(4), 3153 (2017)
111. J. Kim, D.H. Seo, H. Kim, I. Park, J.K. Yoo, S.K. Jung, Y.U. Park, W.A. Goddard, K. Kang, Unexpected discovery of low-cost maricite $NaFePO_4$ as a high-performance electrode for Na-ion batteries. Energy Environ. Sci. **8**(2), 540 (2015)
112. D. Saurel, M. Galceran, M. Reynaud, H. Anne, M. Casas-Cabanas, Rate dependence of the reaction mechanism in olivine $NaFePO_4$ Na-ion cathode material. Int. J. Energy Res. **42**(10), 3258 (2018)
113. F. Zhou, T. Maxisch, G. Ceder, Configurational electronic entropy and the phase diagram of mixed-valence oxides: The case of Li_xFePO_4. Phys. Rev. Lett. **97**(15), 155704 (2006)
114. A. Saracibar, J. Carrasco, D. Saurel, M. Galceran, B. Acebedo, H. Anne, M. Lepoitevin, T. Rojo, M. Casas Cabanas, Investigation of sodium insertion-extraction in olivine Na_xFePO_4 ($0 \le x \le 1$) using first-principles calculations. Phys. Chem. Chem. Phys. **18**(18), 13045 (2016)
115. S.M. Oh, S.T. Myung, J. Hassoun, B. Scrosati, Y.K. Sun, Reversible $NaFePO_4$ electrode for sodium secondary batteries. Electrochem. Commun. **22**(1), 149 (2012)
116. Y. Liu, N. Zhang, F. Wang, X. Liu, L. Jiao, L.Z. Fan, Approaching the downsizing limit of maricite $NaFePO_4$ toward high-performance cathode for sodium-ion batteries. Adv. Funct. Mater. **28**(30), 1801917 (2018)
117. V. Koleva, T. Boyadzhieva, E. Zhecheva, D. Nihtianova, S. Simova, G. Tyuliev, R. Stoyanova, Precursor-based methods for low-temperature synthesis of defectless $NaMnPO_4$ with an olivine- and maricite-type structure. Cryst. Eng. Comm. **15**(44), 9080 (2013)
118. A. Chiring, M. Mazumder, S.K. Pati, C.S. Johnson, P. Senguttuvan, Unraveling the formation mechanism of $NaCoPO_4$ polymorphs. J. Solid State Chem. **293**, 121766 (2021)
119. B. Senthilkumar, K.V. Sankar, L. Vasylechko, Y.S. Lee, R.K. Selvan, Synthesis and electrochemical performances of maricite-$NaMPO_4$ (M = Ni Co, Mn) electrodes for hybrid supercapacitors. RSC Adv. **4**(95), 53192 (2014)
120. O. Kamon-In, W. Klysubun, W. Limphirat, S. Srilomsak, N. Meethong, An insight into crystal, electronic, and local structures of lithium iron silicate (Li_2FeSiO_4) materials upon lithium extraction. Physica B **416**, 69 (2013)
121. S. Yu, J.Q. Hu, M.B. Hussain, S.Q. Wu, Y. Yang, Z.Z. Zhu, Structural stabilities and electrochemistry of Na_2FeSiO_4 polymorphs: First-principles calculations. J. Solid State Electrochem. **22**(7), 2237 (2018)
122. J. Zhang, S.-H. Luo, Q.-X. Ren, D.-J. Zhang, Y. Qin, Tailoring the sodium doped $LiMnPO_4$/C orthophosphate to nanoscale as a high-performance cathode for lithium ion battery. Appl. Surf. Sci. **530**, 146628 (2020)
123. J. Lu, S. Ichi Nishimura, A. Yamada, A Fe-rich sodium iron orthophosphate as cathode material for rechargeable batteries. Electrochem. Commun. **79**, 51 (2017)
124. H. Zhu, J. Wang, X. Liu, X. Zhu, Facile preparation of a Na_2MnSiO_4/C/graphene composite as a high performance cathode for sodium ion batteries. RSC Adv. **7**(23), 14145 (2017)
125. V. Sudarsanan, A.M. Augustine, P. Ravindran, Investigation of electronic structure and electrochemical properties of Na_2MnSiO_4 as a cathode material for Na ion batteries. J. Phys. Chem. C **125**(47), 25968 (2021)
126. V.S. Rangasamy, S. Thayumanasundaram, J.P. Locquet, Solvothermal synthesis and electrochemical properties of Na_2CoSiO_4 and Na_2CoSiO_4/carbon nanotube cathode materials for sodium-ion batteries. Electrochim. Acta **276**, 102 (2018)
127. M. Law, V. Ramar, P. Balaya, Na_2MnSiO_4 as an attractive high capacity cathode material for sodium-ion battery. J. Power Sources **359**, 277 (2017)
128. S.C. Lim, J.T. Vaughey, W.T.A. Harrison, L.L. Dussack, A.J. Jacobson, J.W. Johnson, Solid state redox transformations of

simple vanadium phosphates: The synthesis of ε-$VOPO_4$. Solid State Ionics **84**(3–4), 219 (1996)
129. N. Dupre, J. Gaubicher, T. le Mercier, G. Wallez, J. Angenault, M. Quarton, Positive electrode materials for lithium batteries based on $VOPO_4$. Solid State Ionics **140**(3–4), 209 (2001)
130. N. Dupré, G. Wallez, J. Gaubicher, M. Quarton, Phase transition induced by lithium insertion in α_I- and α_{II}- $VOPO_4$. J. Solid State Chem. **177**(8), 2896 (2004)
131. F. Girgsdies, W.S. Dong, J.K. Bartley, G.J. Hutchings, R. Schlögl, T. Ressler, The crystal structure of ε-$VOPO_4$. Solid State Sci. **8**(7), 807 (2006)
132. E. Bordes, Crystallochemistry of V-P-O phases and application to catalysis. Catal. Today **1**(5), 499 (1987)
133. F. Girgsdies, M. Schneider, A. Brückner, T. Ressler, R. Schlögl, The crystal structure of δ-$VOPO_4$ and its relationship to ω-$VOPO_4$. Solid State Sci. **11**(7), 1258 (2009)
134. P. Amorós, M.D. Marcos, M. Roca, J. Alamo, A. Beltrán-Porter, D. Beltrán-Porter, Crystal structure of a new polytype in the V-P-O system: Is ω-$VOPO_4$ a dynamically stabilised metastable network? J. Phys. Chem. Solids **62**(8), 1393 (2001)
135. P.A. Aparicio, J.A. Dawson, M.S. Islam, N.H. de Leeuw, Computational study of $NaVOPO_4$ polymorphs as cathode materials for Na-ion batteries: Diffusion, electronic properties, and cation-doping behavior. J. Phys. Chem. C **122**(45), 25829 (2018)
136. G. He, A. Huq, W.H. Kan, A. Manthiram, β-$NaVOPO_4$ obtained by a low-temperature synthesis process: A new 3.3 V cathode for sodium-ion batteries. Chem. Mater. **28**(5), 1503 (2016)
137. Y. Fang, Q. Liu, L. Xiao, Y. Rong, Y. Liu, Z. Chen, X. Ai, Y. Cao, H. Yang, J. Xie, C. Sun, X. Zhang, B. Aoun, X. Xing, X. Xiao, Y. Ren, A fully sodiated $NaVOPO_4$ with layered structure for high-voltage and long-lifespan sodium-ion batteries. Chem **4**(5), 1167 (2018)
138. E. Abadila Iffer, M. Belaiche, C.A. Ferdi, M. Elansary, A.K. Sunar, Y. Wang, Y. Cao, Monoclinic α-$NaVOPO_4$ as cathode materials for sodium-ions batteries: Experimental and DFT investigation. Int. J. Energy Res. **45**(2), 1703 (2021)
139. J. Gao, W. Huang, S. Qin, X. Wu, High pressure structural investigation on alluaudites $Na_2Fe_3(PO_4)_3$-$Na_2FeMn_2(PO_4)_3$ system. J. Solid State Chem. **247**, 156 (2017)
140. F. Leroux, A. Mar, D. Guyomard, Y. Piffard, Cation substitution in the alluaudite structure type: Synthesis and structure of $AgMn_3(PO_4)(HPO_4)_2$. J. Solid State Chem. **117**(1), 206 (1995)
141. F. Hatert, P. Keller, F. Lissner, D. Antenucci, A.-M. Fransolet, First experimental evidence of alluaudite-like phosphates with high Li-content: The $(Na_{1-x}Li_x)MnFe_2(PO_4)_3$ series (x = 0 to 1). Eur. J. Mineral. **12**(4), 847 (2000)
142. P. Barpanda, G. Oyama, S.I. Nishimura, S.C. Chung, A. Yamada, A 3.8-V earth-abundant sodium battery electrode. Nat. Commun. **5**, 4358 (2014)
143. K. Trad, D. Carlier, L. Croguennec, A. Wattiaux, M. Ben Amara, C. Delmas, $NaMnFe_2(PO_4)_3$ alluaudite phase: Synthesis, structure, and electrochemical properties as positive electrode in lithium and sodium batteries. Chem. Mater. **22**(19), 5554 (2010)
144. D. Dwibedi, P.W. Jaschin, R. Gond, P. Barpanda, Revisiting the alluaudite $NaMnFe_2(PO_4)_3$ sodium insertion material: Structural, diffusional and electrochemical insights. Electrochim. Acta **283**, 850 (2018)
145. M. Wen, X. Liu, Y. Zhao, S. Liu, H. Liu, Y. Dong, Q. Kuang, Q. Fan, Synthesis of alluaudite-type $Na_2VFe_2(PO_4)_3$/C and its electrochemical performance as cathode material for sodium-ion battery. J. Solid State Electrochem. **22**(3), 891 (2018)
146. R. Essehli, I. Belharouak, H. Ben Yahia, K. Maher, A. Abouimrane, B. Orayech, S. Calder, X.L. Zhou, Z. Zhou, Y.K. Sun, Alluaudite $Na_2Co_2Fe(PO_4)_3$ as an electroactive material for sodium ion batteries. Dalton Trans. **44**(17), 7881 (2015)
147. R. Essehli, I. Belharouak, H. Ben Yahia, R. Chamoun, B. Orayech, B. el Bali, K. Bouziane, X.L. Zhou, Z. Zhou, α-$Na_2Ni_2Fe(PO_4)_3$: A dual positive/negative electrode material for sodium ion batteries. Dalton Trans. **44**(10), 4526 (2015)
148. D. Harbaoui, M.M.S. Sanad, C. Rossignol, E.K. Hlil, N. Amdouni, S. Obbade, Synthesis and structural, electrical, and magnetic properties of new iron-aluminum alluaudite phases β-$Na_2Ni_2M(PO_4)_3$ (M = Fe and Al). Inorg. Chem. **56**(21), 13051 (2017)
149. M. Hadouchi, A. Assani, M. Saadi, I. Saadoune, A. Lahmar, H. Bouyanfif, M. EL Marssi, L. EL Ammari, Synthesis, crystal structure and properties of a new phosphate, $Na_2Co_2Cr(PO_4)_3$. J. Inorg. Organomet. Polym Mater. **28**(6), 2854 (2018)
150. K. Walczak, A. Kulka, J. Molenda, Alluaudite-$Na_{1.47}Fe_3(PO_4)_3$: Structural and electrochemical properties of potential cathode material for Na-ion batteries. Solid State Sci. **87**, 21 (2019)
151. R. Essehli, H. BenYahia, K. Maher, M.T. Sougrati, A. Abouimrane, J.B. Park, Y.K. Sun, M.A. Al-Maadeed, I. Belharouak, Unveiling the sodium intercalation properties in $Na_{1.86\square 0.14}Fe_3(PO_4)_3$. J. Power Sources **324**, 657 (2016)
152. C. Masquelier, L. Croguennec, Polyanionic (phosphates, silicates, sulfates) frameworks as electrode materials for rechargeable Li (or Na) batteries. Chem. Rev. **113**(8), 6552 (2013)
153. R.B. Araujo, S. Chakraborty, P. Barpanda, R. Ahuja, $Na_2M_2(SO_4)_3$ (M = Fe, Mn, Co and Ni): Towards high-voltage sodium battery applications. Phys. Chem. Chem. Phys. **18**(14), 9658 (2016)
154. D. Dwibedi, R. Gond, A. Dayamani, R.B. Araujo, S. Chakraborty, R. Ahuja, P. Barpanda, $Na_{2.32}Co_{1.84}(SO_4)_3$ as a new member of the alluaudite family of high-voltage sodium battery cathodes. Dalton Trans. **46**(1), 55 (2017)
155. D. Dwibedi, R.B. Araujo, S. Chakraborty, P.P. Shanbogh, N.G. Sundaram, R. Ahuja, P. Barpanda, $Na_{2.44}Mn_{1.79}(SO_4)_3$: A new member of the alluaudite family of insertion compounds for sodium ion batteries. J. Mater. Chem. A **3**(36), 18564 (2015)

156. D. Dwibedi, P. Barpanda, Solution-assisted energy-savvy synthesis of high-voltage $Na_2M_2(SO_4)_3$ (M = 3d metals) alluaudite family of sodium insertion materials. J. Power Sources **296**, 276 (2018)
157. D. Dwibedi, C.D. Ling, R.B. Araujo, S. Chakraborty, S. Duraisamy, N. Munichandraiah, R. Ahuja, P. Barpanda, Ionothermal synthesis of high-voltage alluaudite $Na_{2+2x}Fe_{2-x}(SO_4)_3$ sodium insertion compound: Structural, electronic, and magnetic insights. ACS Appl. Mater. Interfaces **8**(11), 6982 (2016)
158. T. Jungers, A. Mahmoud, C. Malherbe, F. Boschini, B. Vertruyen, Sodium iron sulfate alluaudite solid solution for Na-ion batteries: Moving towards stoichiometric $Na_2Fe_2(SO_4)_3$. J. Mater. Chem. A **7**(14), 8226 (2019)
159. A. Plewa, A. Kulka, E. Hanc, W. Zając, J. Sun, L. Lu, J. Molenda, Facile aqueous synthesis of high performance $Na_2FeM(SO_4)_3$ (M = Fe, Mn, Ni) alluaudites for low cost Na-ion batteries. J. Mater. Chem. A **8**(5), 2728 (2020)
160. W. Pan, W. Guan, S. Liu, B. Bin Xu, C. Liang, H. Pan, M. Yan, Y. Jiang, $Na_2Fe_2(SO_4)_3$: An anhydrous 3.6 V, low-cost and good-safety cathode for a rechargeable sodium-ion battery. J. Mater. Chem. A **7**(21), 13197 (2019)
161. T. Watcharatharapong, S. Chakraborty, R. Ahuja, Mapping the sodium intercalation mechanism, electrochemical properties and structural evolution in non-stoichiometric alluaudite $Na_{2+2\delta}Fe_{2-\delta}(SO_4)_3$ cathode materials. J. Mater. Chem. A **7**(29), 17446 (2019)
162. S. Wei, B. MortemarddeBoisse, G. Oyama, S.I. Nishimura, A. Yamada, Synthesis and electrochemistry of $Na_{2.5}(Fe_{1-y}Mn_y)_{1.75}(SO_4)_3$ solid solutions for Na-ion batteries. ChemElectroChem **3**(2), 209 (2016)
163. D.M. Marinova, V.V. Kostov, R.P. Nikolova, R.R. Kukeva, E.N. Zhecheva, R.K. Stoyanova, Redox properties of alluaudite sodium cobalt manganese sulfates as high-voltage electrodes for rechargeable batteries. Chem. Commun. **54**(43), 5466 (2018)
164. P. Barpanda, T. Ye, S.I. Nishimura, S.C. Chung, Y. Yamada, M. Okubo, H. Zhou, A. Yamada, Sodium iron pyrophosphate: A novel 3.0 V iron-based cathode for sodium-ion batteries. Electrochem. Commun. **24**(1), 116 (2012)
165. H. Kim, R.A. Shakoor, C. Park, S.Y. Lim, J.S. Kim, Y.N. Jo, W. Cho, K. Miyasaka, R. Kahraman, Y. Jung, J.W. Choi, $Na_2FeP_2O_7$ as a promising iron-based pyrophosphate cathode for sodium rechargeable batteries: A combined experimental and theoretical study. Adv. Funct. Mater. **23**(9), 1147 (2013)
166. F. Sanz, C. Parada, J.M. Rojo, C. Ruiz-Valero, R. Saez-Puche, Studies on tetragonal $Na_2CoP_2O_7$, a novel ionic conductor. J. Solid State Chem. **145**(2), 604 (1999)
167. P. Barpanda, J. Lu, T. Ye, M. Kajiyama, S.C. Chung, N. Yabuuchi, S. Komaba, A. Yamada, A layer-structured $Na_2CoP_2O_7$ pyrophosphate cathode for sodium-ion batteries. RSC Adv. **3**(12), 3857 (2013)
168. K.-H. Ha, M.-S. Kwon, K.T. Lee, Triclinic $Na_{3.12}Co_{2.44}(P_2O_7)_2$ as a high redox potential cathode material for Na-ion batteries. J. Electrochem. Sci. Technol. **11**(2), 187 (2020)
169. J.M. Clark, P. Barpanda, A. Yamada, M.S. Islam, Sodium-ion battery cathodes $Na_2FeP_2O_7$ and $Na_2MnP_2O_7$: Diffusion behaviour for high rate performance. J. Mater. Chem. A **2**(30), 11807 (2014)
170. P. Barpanda, G. Liu, C.D. Ling, M. Tamaru, M. Avdeev, S.C. Chung, Y. Yamada, A. Yamada, $Na_2FeP_2O_7$: A safe cathode for rechargeable sodium-ion batteries. Chem. Mater. **25**(17), 3480 (2013)
171. R.A. Shakoor, C.S. Park, A.A. Raja, J. Shin, R. Kahraman, A mixed iron-manganese based pyrophosphate cathode, $Na_2Fe_{0.5}Mn_{0.5}P_2O_7$, for rechargeable sodium ion batteries. Phys. Chem. Chem. Phys. **18**(5), 3929 (2016)
172. P. Barpanda, T. Ye, M. Avdeev, S.C. Chung, A. Yamada, A new polymorph of $Na_2MnP_2O_7$ as a 3.6 V cathode material for sodium-ion batteries. J. Mater. Chem. A **1**(13), 4194 (2013)
173. M. Tanabe, T. Honma, T. Komatsu, Unique crystallization behavior of sodium manganese pyrophosphate $Na_2MnP_2O_7$ glass and its electrochemical properties. J. Asian Ceram. Soc. **5**(2), 209 (2017)
174. H. Li, X. Chen, T. Jin, W. Bao, Z. Zhang, L. Jiao, Robust graphene layer modified $Na_2MnP_2O_7$ as a durable high-rate and high energy cathode for Na-ion batteries. Energy Storage Mater. **16**, 383 (2019)
175. H. Kim, C.S. Park, J.W. Choi, Y. Jung, Defect-controlled formation of triclinic $Na_2CoP_2O_7$ for 4 V sodium-ion batteries. Angew. Chem. Int. Ed. **55**(23), 6662 (2016)
176. H.J. Song, J.C. Kim, M.A. Dar, D.W. Kim, Controlled phase stability of highly Na-active triclinic structure in nanoscale high-voltage $Na_{2-2x}Co_{1+x}P_2O_7$ cathode for Na-ion batteries. J. Power Sources **377**, 121 (2018)
177. H. Li, Z. Zhang, M. Xu, W. Bao, Y. Lai, K. Zhang, J. Li, triclinic off-stoichiometric $Na_{3.12}Mn_{2.44}(P_2O_7)_2$/C cathode materials for high-energy/power sodium-ion batteries. ACS Appl. Mater. Interfaces **10**(29), 24564 (2018)
178. Y. Zhang, J. Zhang, X. Li, G. Chen, B. Zhang, H. Liu, Y. Wang, Z.-F. Ma, Construction of AlF3 layer to improve $Na_{3.12}Fe_{2.44}(P_2O_7)_2$ interfacial stability for high temperature stable cycling. Chem. Eng. J. **430**, 132708 (2022)
179. S. Wang, T. Zhu, F. Chen, X. Ding, Q. Hu, J. Liao, X. He, C. Chen, $Cr_2P_2O_7$ as a novel anode material for sodium and lithium storage. Materials **13**(14), 3139 (2020)
180. Y. Wen, L. Chen, Y. Pang, Z. Guo, D. Bin, Y. Gang Wang, C. Wang, Y. Xia, TiP_2O_7 and expanded graphite nanocomposite as anode material for aqueous lithium-ion batteries. ACS Appl. Mater. Interfaces **9**(9), 8075 (2017)
181. P. Serras, V. Palomares, T. Rojo, *Alkali-Ion Batteries, edited by D* (Yang IntechOpen, London, 2016)

182. R. Tripathi, T.N. Ramesh, B.L. Ellis, L.F. Nazar, Scalable synthesis of tavorite $LiFeSO_4F$ and $NaFeSO_4F$ cathode materials. Angew. Chem. Int. Ed. **49**(46), 8738 (2010)
183. M. Ling, Q. Jiang, T. Li, C. Wang, Z. Lv, H. Zhang, Q. Zheng, X. Li, The mystery from tetragonal $NaVPO_4F$ to monoclinic $NaVPO_4F$: Crystal presentation, phase conversion, and Na-storage kinetics. Adv. Energy Mater. **11**(21), 2100627 (2021)
184. J. Zhou, J. Zhou, Y. Tang, Y. Bi, C. Wang, D. Wang, S. Shi, Synthesis of Na_2FePO_4F/C and its electrochemical performance. Ceram. Int. **39**(5), 5379 (2013)
185. D. Chen, G.Q. Shao, B. Li, G.G. Zhao, J. Li, J.H. Liu, Z.S. Gao, H.F. Zhang, Synthesis, crystal structure and electrochemical properties of $LiFePO_4F$ cathode material for Li-ion batteries. Electrochim. Acta **147**, 663 (2014)
186. M. Hellenbrandt, The inorganic crystal structure database (ICSD)—present and future. Crystallogr. Rev. **10**(1), 17 (2004)
187. L. Sharma, P.K. Nayak, E. de La Llave, H. Chen, S. Adams, D. Aurbach, P. Barpanda, Electrochemical and diffusional investigation of $Na_2Fe^{II}PO_4F$ fluorophosphate sodium insertion material obtained from Fe^{III} precursor. ACS Appl. Mater. Interfaces **9**(40), 34961 (2017)
188. I.K. Lee, I.B. Shim, C.S. Kim, Spin ordering between sub-lattices in NASICON $Li_3Fe_2(PO_4)_3$ measured by Mossbauer spectroscopy. J. Appl. Phys. **113**(17), 17E117 (2011)
189. M. Ramzan, S. Leƀgue, P. Larsson, R. Ahuja, Structural, magnetic, and energetic properties of Na_2FePO_4F, Li_2FePO_4F, $NaFePO_4F$, and $LiFePO_4F$ from ab initio calculations. J. Appl. Phys. **106**(4), 43510 (2009)
190. F. Wang, N. Zhang, X. Zhao, L. Wang, J. Zhang, T. Wang, F. Liu, Y. Liu, L.Z. Fan, Realizing a high-performance Na-storage cathode by tailoring ultrasmall Na_2FePO_4F nanoparticles with facilitated reaction kinetics. Adv. Sci. **6**(13), 1900649 (2019)
191. B.L. Ellis, W.R.M. Makahnouk, Y. Makimura, K. Toghill, L.F. Nazar, A multifunctional 3.5V iron-based phosphate cathode for rechargeable batteries. Nat. Mater. **6**(10), 749 (2007)
192. Y. Zheng, P. Zhang, S.Q. Wu, Y.H. Wen, Z.Z. Zhu, Y. Yang, First-principles investigations on the Na_2MnPO_4F as a cathode material for Na-ion batteries. J. Electrochem. Soc. **160**(6), A927 (2013)
193. N.V. Kosova, D.O. Rezepova, $Na_{1+y}VPO_4F_{1+y}$ ($0 \le y \le 0.5$) as cathode materials for hybrid Na/Li batteries. Inorganics **5**(2), 19 (2017)
194. M. Bianchini, N. Brisset, F. Fauth, F. Weill, E. Elkaim, E. Suard, C. Masquelier, L. Croguennec, $Na_3V_2(PO_4)_2F_3$ revisited: A high-resolution diffraction study. Chem. Mater. **26**(14), 4238 (2014)
195. F. Sauvage, E. Quarez, J.M. Tarascon, E. Baudrin, Crystal structure and electrochemical properties vs. Na+ of the sodium fluorophosphate $Na_{1.5}VOPO_4F_{0.5}$. Solid State Sci. **8**(10), 1215 (2006)
196. M. Mazumder, S.K. Pati, Theoretical insights into $Na_5M(PO_4)_2F_2$ (M = Cr, V): A fluorophosphate-based high-performance cathode system for sodium-ion batteries. J. Phys. Chem. C **125**(36), 19593 (2021)
197. J. Barker, M. Saidi, J. Swoyer, Sodium ion batteries. *US20020192553A1* (2002)
198. R.A. Shakoor, D.-H. Seo, H. Kim, Y.-U. Park, J. Kim, S.-W. Kim, H. Gwon, S. Lee, K. Kang, A combined first principles and experimental study on $Na_3V_2(PO_4)_2F_3$ for rechargeable Na batteries. J. Mater. Chem. **22**(38), 20535 (2012)
199. S.T. Dacek, W.D. Richards, D.A. Kitchaev, G. Ceder, Structure and dynamics of fluorophosphate Na-ion battery cathodes. Chem. Mater. **28**(15), 5450 (2016)
200. G. Yan, S. Mariyappan, G. Rousse, Q. Jacquet, M. Deschamps, R. David, B. Mirvaux, J.W. Freeland, J.-M. Tarascon, Higher energy and safer sodium ion batteries via an electrochemically made disordered $Na_3V_2(PO_4)_2F_3$ material. Nat. Commun. **10**(1), 585 (2019)
201. M. Bianchini, F. Fauth, N. Brisset, F. Weill, E. Suard, C. Masquelier, L. Croguennec, Comprehensive investigation of the $Na_3V_2(PO_4)_2F_3$–$NaV_2(PO_4)_2F_3$ system by operando high resolution synchrotron X-ray diffraction. Chem. Mater. **27**(8), 3009 (2015)
202. C. Zhu, C. Wu, C.-C. Chen, P. Kopold, P.A. van Aken, J. Maier, Y. Yu, A High power-high energy $Na_3V_2(PO_4)_2F_3$ sodium cathode: Investigation of transport parameters, rational design and realization. Chem. Mater. **29**(12), 5207 (2017)
203. K. Kawai, D. Asakura, S. Nishimura, A. Yamada, 4.7 V operation of the Cr^{4+}/Cr^{3+} redox couple in $Na_3Cr_2(PO_4)_2F_3$. Chem. Mater. **33**(4), 1373 (2021)
204. L.H.B. Nguyen, A. Iadecola, S. Belin, J. Olchowka, C. Masquelier, D. Carlier, L. Croguennec, A combined operando synchrotron X-ray absorption spectroscopy and first-principles density functional theory study to unravel the vanadium redox paradox in the $Na_3V_2(PO_4)_2F_3$–$Na_3V_2(PO_4)_2FO_2$ compositions. J. Phys. Chem. C **124**(43), 23511 (2020)
205. T. Broux, T. Bamine, F. Fauth, L. Simonelli, W. Olszewski, C. Marini, M. Ménétrier, D. Carlier, C. Masquelier, L. Croguennec, Strong impact of the oxygen content in $Na_3V_2(PO_4)_2F_{3-y}O_y$ ($0 \le y \le 0.5$) on its structural and electrochemical properties. Chem. Mater. **28**(21), 7683 (2016)
206. P. Barpanda, C.D. Ling, G. Oyama, A. Yamada, Sodium manganese fluorosulfate with a triplite structure. Acta Crystallogr. Sect. B **69**(6), 584 (2013)
207. P. Barpanda, J.-N. Chotard, N. Recham, C. Delacourt, M. Ati, L. Dupont, M. Armand, J.-M. Tarascon, Structural, transport, and electrochemical investigation of novel $AMSO_4F$ (A = Na, Li; M = Fe Co, Ni, Mn) metal fluorosulphates prepared using low temperature synthesis routes. Inorg. Chem. **49**(16), 7401 (2010)
208. R. Tripathi, G.R. Gardiner, M.S. Islam, L.F. Nazar, Alkali-ion conduction paths in $LiFeSO_4F$ and $NaFeSO_4F$ tavorite-type cathode materials. Chem. Mater. **23**(8), 2278 (2011)

209. R. Rajagopalan, Z. Wu, Y. Liu, S. Al-Rubaye, E. Wang, C. Wu, W. Xiang, B. Zhong, X. Guo, S.X. Dou, H.K. Liu, A novel high voltage battery cathodes of Fe^{2+}/Fe^{3+} sodium fluoro sulfate lined with carbon nanotubes for stable sodium batteries. J. Power Sources **398**, 175 (2018)
210. J. Liang, Y. Li, X. Hou, F. Wang, W. Zhang, J. Zhang, S. Tang, H. Sun, Insight into electrochemical and elastic properties in $AFe_{1-x}M_xSO_4F$ (A = Li, Na; M = Co, Ni, Mg) cathode materials: A first principle study. Electrochim. Acta **251**, 316 (2017)
211. G. Sai Gautam, E.B. Stechel, E.A. Carter, Exploring Ca-Ce-M-O (M = 3d transition metal) oxide perovskites for solar thermochemical applications. Chem. Mater. **32**(23), 9964 (2020)
212. Y. Han, J. Hu, C. Yin, Y. Zhang, J. Xie, D. Yin, C. Li, Iron-based fluorides of tetragonal tungsten bronze structure as potential cathodes for Na-ion batteries. J. Mater. Chem. A **4**(19), 7382 (2016)
213. C. Zhang, S. An, W. Li, H. Xu, W. Hao, W. Liu, Z. Li, X. Qiu, Hierarchical mesoporous iron fluoride and reduced graphene oxide nanocomposite as cathode materials for high-performance sodium-ion batteries. ACS Appl. Mater. Interfaces **12**(15), 17538 (2020)
214. U.K. Dey, N. Barman, S. Ghosh, S. Sarkar, S.C. Peter, P. Senguttuvan, Topochemical bottom-up synthesis of 2D- and 3D-sodium iron fluoride frameworks. Chem. Mater. **31**(2), 295 (2019)
215. A. Martin, M.L. Doublet, E. Kemnitz, N. Pinna, Reversible sodium and lithium insertion in iron fluoride perovskites. Adv. Funct. Mater. **28**(29), 1802057 (2018)
216. D. Cao, C. Yin, D. Shi, Z. Fu, J. Zhang, C. Li, Cubic perovskite fluoride as open framework cathode for Na-ion batteries. Adv. Funct. Mater. **27**(28), 1701130 (2017)
217. J. Liao, J. Han, J. Xu, Y. Du, Y. Sun, L. Duan, X. Zhou, Scalable synthesis of Na_2MVF_7 (M = Mn, Fe, and Co) as high-performance cathode materials for sodium-ion batteries. Chem. Commun. **57**(87), 11497 (2021)
218. E.E. Foley, A. Wong, R.C. Vincent, A. Manche, A. Zaveri, E. Gonzalez-Correa, G. Ménard, R.J. Clément, Probing reaction processes and reversibility in Earth-abundant Na_3FeF_6 for Na-ion batteries. Phys. Chem. Chem. Phys. **23**(36), 20052 (2021)
219. N. Dimov, A. Nishimura, K. Chihara, A. Kitajou, I.D. Gocheva, S. Okada, Transition metal $NaMF_3$ compounds as model systems for studying the feasibility of ternary Li-M-F and Na-M-F single phases as cathodes for lithium-ion and sodium-ion batteries. Electrochim. Acta **110**, 214 (2013)
220. C. Bohnke, J.L. Fourquet, N. Randrianantoandro, T. Brousse, O. Crosnier, Electrochemical intercalation of lithium into the perovskite-type NbO_2F: Influence of the NbO_2F particle size. J. Solid State Electrochem. **5**(1), 1 (2001)
221. K. Mukai, T. Uyama, I. Yamada, Electrochemical properties of chromium oxyfluoride $CrO_{2-x}F_x$ with $0 \le x \le 0.3$. Inorg. Chem. Front. **6**(11), 3196 (2019)
222. M. Sina, K.-W. Nam, D. Su, N. Pereira, X.-Q. Yang, G.G. Amatucci, F. Cosandey, Structural phase transformation and Fe valence evolution in FeO_xF_{2-x}/C nanocomposite electrodes during lithiation and de-lithiation processes. J. Mater. Chem. A **1**(38), 11629 (2013)
223. A. Kitajou, L. Zhao, R. Nagano, A. Inoishi, E. Kobayashi, S. Okada, Electrochemical performance and thermal stability of iron oxyfluoride (FeOF) for sodium-ion batteries. Batteries **4**(4), 68 (2018)
224. N. Pereira, F. Badway, M. Wartelsky, S. Gunn, G.G. Amatucci, Iron oxyfluorides as high capacity cathode materials for lithium batteries. J. Electrochem. Soc. **156**(6), A407 (2009)
225. D. Chen, J. Ahn, E. Self, J. Nanda, G. Chen, Understanding cation-disordered rocksalt oxyfluoride cathodes. J. Mater. Chem. A **9**(12), 7826 (2021)
226. R.J. Clément, Z. Lun, G. Ceder, Cation-disordered rocksalt transition metal oxides and oxyfluorides for high energy lithium-ion cathodes. Energy Environ. Sci. **13**(2), 345 (2020)
227. M. Chen, D. Cortie, Z. Hu, H. Jin, S. Wang, Q. Gu, W. Hua, E. Wang, W. Lai, L. Chen, S.L. Chou, X.L. Wang, S.X. Dou, A novel graphene oxide wrapped $Na_2Fe_2(SO_4)_3$/C cathode composite for long life and high energy density sodium-ion batteries. Adv. Energy Mater. **8**(27), 1800944 (2018)
228. Z. Wang, S. Park, Z. Deng, D. Carlier, J.-N. Chotard, L. Croguennec, G.S. Gautam, A.K. Cheetham, C. Masquelier, P. Canepa, Phase stability and sodium-vacancy orderings in a NaSICON electrode. J. Mater. Chem. A **10**(1), 209 (2022)
229. S. Park, Z. Wang, Z. Deng, I. Moog, P. Canepa, F. Fauth, D. Carlier, L. Croguennec, C. Masquelier, J.-N. Chotard, Crystal structure of $Na_2V_2(PO_4)_3$, an intriguing phase spotted in the $Na_3V_2(PO_4)_3$-$Na_1V_2(PO_4)_3$ system. Chem. Mater. **34**(1), 451 (2022)